Expansion and intensification of the North American Monsoon during the Pliocene

- Tripti Bhattacharya ¹, Ran Feng ², Jessica E. Tierney ³, Claire Rubbelke, ¹, Natalie Burls ⁴,

 Scott Knapp ⁴, Minmin Fu ⁵
- ¹Department of Earth and Environmental Sciences, Syracuse University, Syracuse NY
- ²Department of Geosciences, University of Connecticut, Storrs CT
- ³Department of Geosciences, University of Arizona, Tucson AZ
- ⁴Department of Atmospheric, Oceanic and Earth Sciences, George Mason University, Fairfax VA
 - ⁵Department of Earth and Planetary Sciences, Harvard University, Cambridge, MA

Key Points:

10

12

14

- Leaf wax hydrogen isotopes preserved in ocean sediments reveal evidence of a stronger mid-Pliocene monsoon in southwestern North America
 - Isotope-enabled simulations show that a stronger monsoon resulted from a diminished east Pacific subtropical-tropical temperature gradient
- This mechanism is relevant to understanding present-day monsoon variability in response to California margin marine heat waves

Corresponding author: Tripti Bhattacharya, trbhatta@syr.edu

Abstract

17

18

19

20

22

23

24

26

27

28

29

31

32

33

34

35

36

37

38

40

41

42

43

45

46

47

48

Southwestern North America, like many subtropical regions, is predicted to become drier in response to anthropogenic warming. However, during the Pliocene, when carbon dioxide was above pre-industrial levels, multiple lines of evidence suggest that southwestern North America was much wetter. While existing explanations for a wet Pliocene invoke increases in winter rain, recent modeling studies hypothesize that summer rain may have also played an important role. Here, we present the first direct evidence for an intensified mid-Pliocene monsoon in southwestern North America using leaf wax hydrogen isotopes. These new records provide evidence that the mid-Pliocene featured an intensified and expanded North American Monsoon. Using proxies and isotope-enabled model simulations, we show that monsoon intensification is linked to amplified warming on the southern California margin relative to the tropical Pacific. This mechanism has clear relevance for understanding present-day monsoon variations, since we show that intervals of amplified subtropical warming on the California margin, as are seen during modern California margin heat waves, are associated with a stronger monsoon. Because marine heat waves are predicted to increase in frequency, the future may bring intervals of 'Pliocene-like' rainfall that co-exist with intensifying megadrought in southwestern North America, with implications for ecosystems, human infrastructure, and water resources.

Plain Language Summary

The middle Pliocene, an interval approximately 3 million years ago, has long puzzled climate scientists. Despite having higher-than-preindustrial carbon dioxide levels, which should result in drier conditions in subtropical regions, some subtropical regions were wet during the Pliocene. In southwestern North America, there were large permanent lakes and plant and animal species that cannot exist in arid regions. We used measurements of hydrogen isotopes in ancient plant matter to show that wet conditions in the Pliocene southwest resulted from a stronger monsoon. This stronger monsoon was caused by changes in subtropical and tropical ocean temperatures in the eastern Pacific. This study presents the first direct evidence that monsoon changes caused wet conditions in the middle Pliocene. It also has relevance for the present, since we find evidence that present-day changes in subtropical ocean temperatures can amplify the monsoon, via a mechanism that strongly resembles what happened in the Pliocene. Our study suggests that further studies of the Pliocene can shed light on how future monsoon changes may influence wildfire, landscapes, and water resources across the southwest.

Introduction

49

50

51

54

55

56

59

60

61

62

65

66

69

70

71

72

73

74

75

76

78

79

80

81

82

83

84

Multiple lines of evidence suggest that southwestern North America (SWNA), like many subtropical continents, was much wetter during the Pliocene epoch, a climate interval featuring reduced ice volume and CO₂ concentrations above preindustrial levels (Figure 1). Sedimentological data document widespread perennial and ephemeral lakes in southern California and Arizona (M. Pound et al., 2014; Ibarra et al., 2018) (Figure 1), and palynological and macrobotanical evidence from southern California suggests expanded tree cover and the presence of species that today only grow in regions with mesic conditions and summer rainfall (Remeika et al., 1988; Ballog & Malloy, 1981). Faunal remains from Baja California contain *Crocodylus* spp. fossils, which require freshwater habitats, further suggesting increased water resources in regions that are arid at present (Salzmann et al., 2009; Miller, 1980). At face value, this evidence for a wet Pliocene is at odds with the theoretical and model-derived prediction that regions like SWNA, and subtropical continents more broadly, will continue to dry in coming centuries as a result of elevated greenhouse gases (Byrne & O'Gorman, 2015; Seager et al., 2010).

Two dominant hypotheses have been proposed to explain the evidence for wet conditions in SWNA during the Pliocene. On a global scale, a dramatically weaker meridional sea surface temperature (SST) gradient could have weakened mean atmospheric circulation and reduced subtropical moisture divergence (Burls & Fedorov, 2017; A. V. Fedorov et al., 2015). However, current proxy-based estimates of SST patterns suggest that reductions in Pliocene meridional gradients were modest (Tierney et al., 2019). Another possibility is that a weaker Pacific Walker circulation shifted winter storm tracks southward, bringing increased moisture to SWNA, similar to what occurs during El Niño events today (Ibarra et al., 2018; Molnar & Cane, 2002). However, this hypothesis would require almost two-fold increases in winter rainfall to explain Pliocene lake distributions, and cannot explain the presence of tree species like Castanea and Carya or the expansion of Sonoran desert flora, which are interpreted as indicators of summer rainfall (Ibarra et al., 2018; Ballog & Malloy, 1981; Axelrod, 1948). These qualitative data suggest a role for the North American Monsoon (NAM), which is the primary source of summer rainfall in the SWNA and maintains the floristically diverse ecosystems of the Sonoran Desert (Cook & Seager, 2013). Today, the NAM is restricted to southern Arizona, New Mexico and northwestern Mexico along the eastern side of the Gulf of California, although summertime convective activity associated with the NAM can extend into southern California. The seasonal cycle of the NAM coincides with the development of an upper level anticyclone over the southwest (Higgins et al., 1998). This circulation primarily derives moisture from the Gulf of California and the tropical eastern Pacific (Barron et al., 2012; Douglas & Leal, 2003), suggesting that SST changes in these regions may strongly influence the strength of the monsoon.

85

86

87

90

91

92

93

95

96

97

100

101

102

103

105

106

107

108

109

110

111

112

114

115

116

117

119

120

A recent modeling study found that warm coastal temperatures on the California margin, similar to those observed in Pliocene proxy records, results in an expansion of summer rainfall across SWNA (Fu et al., 2022). In these simulations, precipitation rates associated with a stronger monsoon exceed evaporation. If these changes are realistic, they suggest that monsoon changes alone could explain the mesic vegetation and high lake levels found in the Pliocene. However, the hypothesis that the NAM was stronger during the Pliocene, an interval characterized by higher greenhouse gas forcing, is at odds with some model predictions of how the NAM responds to higher atmospheric greenhouse gases (Pascale et al., 2017).

Current-generation models do not show consensus about the response of the NAM to 21st century warming, possibly as a result of systematic biases and low resolution that prevents many models from accurately capturing California Margin and Gulf of California SSTs (Maloney et al., 2014; Meyer & Jin, 2017; Cook & Seager, 2013; Almazroui et al., 2021; Moon & Ha, 2020). A recent high-resolution modeling study with a bias-corrected SST field suggests that the NAM will weaken in response to 21st century warming. In this simulation, the NAM strength responds to the *relative* warming of SST in the subtropical eastern Pacific (e.g. southern California Margin) (Pascale et al., 2017). Specifically, because the southern California margin warms at a slower rate than the tropical eastern equatorial Pacific (EEP), SWNA experiences stronger descending motion and greater atmospheric stability, reducing NAM convection. This strong sensitivity to SST gradients distinguishes the NAM from other monsoons, which respond more strongly to direct CO2 forcing. This conceptual model, similar to the 'warmerget-wetter' paradigm (Xie et al., 2010), suggests that past and future NAM strength depends less on the absolute magnitude of warming on the southern California Margin, as suggested by (Fu et al., 2022), but instead depends on the gradient of temperature between the subtropical eastern Pacific and the tropical eastern Pacific. This latter conceptual model has been applied to understanding NAM variations over the Holocene (Barron et al., 2012).

In light of this uncertainty, continuous Plio-Pleistocene, summer rainfall-sensitive proxy records are invaluable for identifying the mechanisms that control long-term changes in NAM rainfall. However, much of the existing proxy evidence from the Pliocene consists of non-continuous snapshots of Pliocene climate, or proxies that can only be interpreted in a purely qualitative framework. Here, we remedy this by presenting the first continuous Plio-Pleistocene records of NAM region hydroclimate, based on leaf wax biomarkers in two marine sediment cores. We focus on reconstructing hydroclimate between the mid-Pliocene, beginning at approximately 3.5 Ma, through the late Pleistocene, although the processes we explore may apply to the broader Pliocene epoch. DSDP 475 is located near the tip of southern Baja California, immediately west of the core modern NAM domain. Our second site, ODP 1012 is on the CA margin, northwest of the NAM domain in the present climatology, and receives virtually no monsoon rain-

fall today. Together, these sites are especially sensitive to hydroclimate changes in the core monsoon domain (DSDP 475), as well as any potential expansion of the monsoon into peripheral zones (ODP 1012). Previous work has shown that the hydrogen isotopic signature of terrestrial plant epicuticular waxes (δD_{wax}) reflects the δD signature of precipitation (δD_p) across a range of ecosystem types (Sachse et al., 2012), and in SWNA, leaf wax δD is strongly sensitive to the relative contribution of monsoonal deep convection to annual rainfall totals (Bhattacharya et al., 2018). This proxy is therefore well-suited for investigating whether summer rainfall played a role in driving Plio-Pleistocene hydroclimatic change. Carbon isotopes provide complementary information by recording shifts in ecosystem composition that influence the magnitude of the offsets between δD_{wax} and δD_p (Figure S1). Our approach therefore allows us to identify changes in monsoon strength and spatial extent over the Plio-Pleistocene.

Materials and Methods

Site Background

DSDP 475 (23.05°N, 109.05°W) is located within the Gulf of California near the south-eastern edge of the peninsula of Baja California (Figure 1). Today, the site sits on a passive continental margin at a water depth of 2631 meters (Curray et al., 1982). This region of Baja California experiences northwesterly wind stress in winter and spring (Zaytsev et al., 2003). In summer, the region around DSDP 475 is influenced by northward advection of waters from the eastern Pacific warm pool (Zaytsev et al., 2003; Durazo & Baumgartner, 2002). The Plio-Pleistocene portion of the core from DSDP 475 is predominantly composed of hemipelagic muds, transitioning to diatomaceous muds in the mid- to early-Pliocene section, showing evidence of a consistent marine setting for this site from the early Pliocene through the Pleistocene (Curray et al., 1982). Age control primarily comes from biostratigraphic tiepoints (Brennan et al., 2022).

ODP 1012 (32.3°N,118.4°W) is located on the California Margin, in the east Cortes Basin, with a water depth of 1772 m. This site experiences northwesterly wind stress year round. The sedimentary section consists of interbedded silty clay, nannofossil mixed sediment, nannofossil ooze (Ostertag-Henning & Stax, 2000). We sample primarily from core 1012A, with supplementary samples from 1012B in the late Pleistocene, to generate a composite Plio-Pleistocene record of climate change. The age model, previously published in J. LaRiviere (2007), is based on δ^{18} O of benthic foraminifera until approximately 1.8 Ma, and thereafter on biostratigraphic tiepoints (T. Herbert et al., 2001).

Leaf Wax Extraction and Measurement

Approximately 100 samples were processed from each of DSDP 475 and ODP 1012, so that the average time interval between samples was 40 kyr for DSDP 475 and 30 kyr for ODP 1012. Leaf waxes were processed via standard methods involving extraction of the total lipid extract (TLE) and purification via column chromatography (Bhattacharya et al., 2018). Following previous work in the region, we focus our analyses on the C_{30} fatty acid, which exclusively derives from terrestrial plants (Bhattacharya et al., 2018).

Concentrations of C_{30} FAMEs, fatty acid methyl esters, were determined using a Trace 1310 GC-FID, and their hydrogen and carbon isotopic composition were measured via gas chromatography isotope ratio mass spectrometry (GC-IR-MS) using a Thermo Delta V Plus mass spectrometer coupled to a Trace 1310 GC-FID, using either a pyrolysis (H₂) or combustion reactor (CO₂). H₂ and CO₂ gases calibrated to a *n*-alkane standard (A7 mix provided by Arndt Schimmelmann at Indiana University) provided references for each analysis. An internal isotopic standard consisting of a synthetic mix of FAMEs was analyzed every 5-7 samples to monitor drift. Samples were run in triplicate for δ D to obtain a precision better than 2% (1σ), and in duplicate or triplicate for δ 13C to obtain a precision better than 0.2% (1σ). While we initially corrected for ice volume changes using a million-year smoothed version of the benthic oxygen isotope stack (Lisiecki & Raymo, 2005) following the method of (Schrag et al., 1996), this correction had a minimal influence on each record (Figure S1), and was omitted in our final analysis.

Inference of Precipitation δD

We leverage paired measurements of carbon and hydrogen isotopes of the C_{30} fatty acid (hereafter, referred to as $\delta^{13}C_{wax}$ and δD_{wax}) to infer the hydrogen isotopic signature of precipitation, or δD_p . δD_{wax} values are offset from the hydrogen isotopic signature of the environmental waters, assumed to be the isotopic value of mean annual precipitation or δD_p . This apparent fractionation or ε_{p-w} varies across plant clades. Graminoids (e.g. grasses) tend to have a larger ε_{p-w} , or are more depleted relative to δD_p , than eudicots, likely reflecting differences in leaf wax biosynthesis and leaf development (Gao et al., 2014). Following previous work, we use $\delta^{13}C_{wax}$ and a Bayesian mixing model (Tierney et al., 2017) to infer the proportion of waxes that come from C_4 grasses in each sample, since C_4 plants have a more enriched carbon isotopic signature than C_3 plants (Collister et al., 1994). End-member constraints on C_4 grasses and C_3 eudicots come from modern plant waxes measured at the Arizona-Sonora Desert Museum in Tucson, AZ (Table S2, S3). These values are based on repeated measurement of new growth on each plant once a month for a calendar year. In order to make measurement of new growth on each plant once a month for a calendar year.

surements more comparable to Plio-Pleistocene leaf wax carbon isotopes, modern plant $\delta^{13}C_{wax}$ measurements were corrected for the Suess effect.

We then use the proportion of inferred C_4 vegetation to determine the appropriate ε_{p-w} to apply to a given sample. Constraints on ε_{p-w} are obtained from δD_{wax} measured on the Arizona-Sonora Desert Museum modern plants. The approach involves weighting the value of ε_{p-w} for C_3 and C_4 plants by the inferred fraction of C_3 and C_4 plants in the sample (Eq. 1).

$$\varepsilon = f_{C4} \cdot \varepsilon_{C4} + (1 - f_{C4}) \cdot \varepsilon_{C3} \tag{1}$$

Finally, our weighted value of ε_{p-w} is used to infer δD_p (Eq. 2).

$$\delta D_{precip} = \frac{1000 + \delta D_{wax}}{(\varepsilon/1000) + 1} - 1000 \tag{2}$$

Because all calculations are performed in a Bayesian framework, uncertainties are propagated through all steps of the calculation. While our initial 1σ precision for δD_w measurements is 2%, 1σ uncertainty for our final estimate of δD_p is 4-6%. This Bayesian approach has been previously used to study paleohydrological signals in leaf waxes (Tierney et al., 2017; Windler et al., 2021), including within the NAM domain (Bhattacharya et al., 2018).

SST Compilation

To identify relationships between leaf wax-inferred δD_p and Plio-Pleistocene changes in large-scale circulation over the north Pacific, we compiled available continuous alkenone-based records of Plio-Pleistocene temperatures from the northeast Pacific. Records were calibrated using BAYSPLINE, a Bayesian calibration that accounts for the attenuation of the relationship between the alkenone unsaturation index and temperature at warmer temperatures (Tierney & Tingley, 2018).

We calculate three indices of Plio-Pleistocene SSTs. First, we calculate average eastern equatorial Pacific SST by taking the mean SST anomaly of sites in the eastern equatorial Pacific including sites IODP U1337, ODP 847, ODP 846, and ODP 1239 (Liu et al., 2019; Dekens et al., 2007; Seki et al., 2012; Rousselle et al., 2013; Shaari et al., 2013; Etourneau et al., 2010; T. D. Herbert et al., 2016; Lawrence et al., 2006). We also exclude the lower resolution record from IODP U1338, although the choice to include or omit this record does not significantly alter our results. Next, we calculate average southern California margin SSTs by taking the average anomaly at sites ODP 1012, ODP 1014, and ODP 1010 (J. P. LaRiviere et al., 2012; J. LaRiviere, 2007; Brierley et al., 2009b; Dekens et al., 2007), also excluding sites with alkenone

records that do not extend to 3.6 Ma (e.g. site 475). Finally, we calculate an index of the subtropical/tropical gradient in the eastern Pacific by subtracting tropical eastern equatorial Pacific SSTs from subtropical southern California Margin SST. This index helps quantify the *relative* warmth on the southern California margin, and is between -7° C and -8° C in the present-day climatology.

Isotope-Enabled Model Simulations

To investigate the drivers of SWNA δD_p changes during the Pliocene, we analyzed simulations conducted with the isotopologue-tracking enabled Community Earth System Model 1.2 (iCESM1.2) in atmosphere-only mode (e.g. iCAM5) (Brady et al., 2019). The atmospheric model is run at a $0.9^{\circ} \times 1.25^{\circ}$ horizontal resolution, with 30 vertical layers. The pre-industrial simulation of iCESM1.2 used in this study captures a similar seasonal cycle of water isotopes compared to GNIP observations, with an enriched summer monsoon compared to depleted winter rainfall (Figure S6), despite the fact that iCESM1.2's rainfall isotopes are depleted compared to observations at Tucson's GNIP station (Nusbaumer et al., 2017). In addition, iCAM5 performs slightly better than other models at simulating rainfall isotope changes due to changing stratiform fraction (Hu et al., 2018).

We prescribe the idealized SST field used in Fu et al. (2022), which is based on the PRISM3 SST reconstruction (Dowsett et al., 2009), but increases temperatures on the southern California Margin to match proxy evidence. All other boundary conditions (e.g. topography, land surface conditions), including CO₂, are kept at pre-industrial values. This simplified experimental design allows us to cleanly isolate the influence of an altered SST field on SWNA hydroclimate.

We also perform 6 additional iCAM5 simulations with different SST patterns and Pliocene boundary conditions in order to better understand the drivers of NAM changes. These simulations featured two types of experiments: in one, we uniformly warm global SSTs without changing the subtropical/tropical gradient in the eastern Pacific. In the other, we incrementally reduce the subtropical/tropical gradient by warming the CA coast. These two sets of experiments identify whether uniform warming of the tropical/subtropical ocean, or alternatively, a changing warming pattern, is more important for driving NAM changes, and should be regarded as sensitivity tests. Simulations are run for 40 years and the last 20 years of model runs are averaged to generate climatologies. It should also be noted that all simulations have fixed atmospheric CO₂ concentrations at Pliocene levels of 400 ppm, resulting in a warmer troposphere with higher evaporative demand. For further details, see Text S1 and Table S4.

Results and Discussion

Plio-Pleistocene Trajectory of δD_p in SWNA

Our new leaf wax-based reconstructions of δD_p indicate a large shift in SWNA hydroclimate between 3.0 and 2.4 Ma, right at the Plio-Pleistocene transition and coinciding with the intensification of Northern Hemisphere glaciation (Figure 1). At site 1012, δD_p is ca. -20 to -40% between 3.5 and 3.0 Ma and then declines to ca. -50 to -60% by 2.5 Ma. After this point, δD_p fluctuates between -65 and -45%. A similar pattern of change is recorded at DSDP 475. At this site, Pliocene values of δD_p range between -45 and -35%, 20 to 35% more enriched than late Pleistocene values. The most enriched values of δD_p occur between 3.5 and 2.9 Ma (Figure 1), after which inferred δD_p values progressively decline until 2.4 Ma. Thereafter, values of δD_p at site 475 show an increase in variability. The increase in variability in the Pleistocene portion of both records likely reflect glacial-interglacial variability. Southward shifts in the westerlies during glacial periods weaken the NAM by promoting 'ventilation' or the import of cold, dry air into the monsoon domain (Bhattacharya et al., 2018).

The similar trajectory of δD_p change over the Plio-Pleistocene transition at both sites suggests that our δD_p reconstructions reflect large-scale reorganizations of hydroclimate rather than any local topographic effects. Furthermore, independent evidence suggests that topography in western North America was already sufficiently high to establish modern circulation patterns and block Gulf of Mexico moisture, making it unlikely that Pliocene δD_p changes reflect an increasing contribution of easterly moisture sources from the Atlantic to coastal regions of Baja and southern California (Mix et al., 2019; Wheeler et al., 2016).

We interpret the enrichment of δD_p in the Pliocene relative to late Pleistocene values as reflecting a greater proportion of convective summer rainfall during this epoch. Summer monsoon rainfall forms from vapor that is rapidly lifted from a warm, saturated boundary in strong convective updrafts (Text S2; Figure S2). This results in an enriched isotopic signature relative to winter moisture, which primarily derives from stratiform precipitation (Aggarwal et al., 2016) (Figure S2). Thus, intervals in time with enhanced deep convective and monsoon rainfall exhibit more enriched values of δD_p . This interpretation differs from the so-called 'amount-effect' observed in other parts of the tropics, and instead reflects the distinct climatology of the NAM region, which features a high proportion of stratiform rainfall in comparison to other monsoon regions (e.g. the Indian monsoon) (Schumacher & Houze, 2003).

Further support for the view that fluctuations in δD_p reflect proportions of convective and stratiform rainfall comes from the fact that spatial gradients in modern coretop leaf wax-inferred δD_p in the Gulf of California show a strong positive correlation with the fraction of rainfall derived from deep convection (Figure S2). Increasing proportions of deep convection

in the region stretching from Baja California to the southern California margin can therefore explain a more positive leaf wax δD_p signature during the Pliocene. This complements the argument made in Bhattacharya et al. (2018), who found that δD_p reflects changing proportions of summer and winter rainfall: summer rainfall is primarily deep convective and winter/spring rainfall derives from stratiform rain (Figure S2). Other processes, like equilibrium temperature effects, are too small to explain the full magnitude of the δD changes (see Text S2).

284

285

286

287

289

290

291

292

293

294

295

296

297

299

300

301

303

304

305

306

307

308

309

310

311

313

314

315

316

In the present climatology, the region around DSDP 475 receives less than 1 mm/day of rain on average, and in many years receives no monsoon rainfall (Fonseca-Hernandez et al., 2021) (Figure S3). A positive Pliocene leaf wax δD_p signature at DSDP 475 likely reflects intensification of the monsoon in its core region, on the slopes of the Sierra Madre Occidental, as well as its expansion into Baja. Similarly, the majority of rain at ODP 1012 in the present day derives from winter moisture, with virtually no contribution from summertime rainfall. The enriched signature of δD_p in the Pliocene at site 1012 reflects a fundamentally different climatology, with a greater proportion of summer rainfall. The similarity of the pattern between DSDP 475 and and ODP 1012 suggests that the latter site reflects the expansion of the NAM into southern California in the Pliocene. This coheres with existing qualitative inferences from southern California palynological data and faunal remains, which suggest that the Pleistocene marked a transition from summer-wet to summer-dry environments in both southern California and Baja California, (Miller, 1980; Ballog & Malloy, 1981; Axelrod, 1948). Together, these lines of evidence suggest that the Pliocene featured a stronger North American Monsoon that was spatially more extensive, influencing the entire region stretching from Baja California through southern California. Moreover, evidence for a warmer and wetter climate in the NAM region is also shown by paleo-botanical evidence from the Miocene (M. J. Pound et al., 2012), suggesting that other warm climate intervals in Earth history also featured a stronger NAM.

SST Patterns and Plio-Pleistocene Monsoon Changes

A recent modeling study hypothesized that warmer California margin temperatures in the Pliocene resulted in expanded and enhanced summer convection (Fu et al., 2022). This hypothesis implies that the evolution of the Plio-Pleistocene NAM should track coastal temperatures on the California Margin. In contrast, other modeling studies suggest that NAM strength responds most strongly to the *relative* warming of the subtropical eastern Pacific (e.g. California Margin) compared to the eastern equatorial Pacific (EEP) (Pascale et al., 2017). To assess the importance of each of these factors in driving NAM changes, we compare our records of summer convection to an index of the eastern Pacific subtropical/tropical temperature gradient, as well as an index of California margin SSTs (see Materials and Methods).

Our Plio-Pleistocene records of SWNA δD_p show a stronger relationship with the eastern Pacific subtropical/tropical gradient than the absolute magnitude of warming on the CA margin (Figure 1e and f). The subtropical/tropical gradient index shows that the temperature difference between the the California Margin and the EEP was at a minimum between 3.5 and 3.0 Ma, and then progressively increased between 3.0 and 2.4 Ma until reaching modern values, where the southern California Margin is approximately 7.6°C cooler than the EEP (Figure 1e). The largest changes in this gradient coincide temporally with the step-like transition to more depleted values in both of our δD_p records (Figure 1). In contrast, southern CA margin temperatures show a gradual long-term decline from 3.5 to 0.8 Ma, with no indication of a step change at the Plio-Pleistocene transition (Figure 1f).

CA margin temperatures and the eastern Pacific subtropical/tropical gradient index are not independent metrics, as the former is used to calculate the latter. However, the temporal evolution of SWNA δD_p more closely mirrors the trajectory of the subtropical-tropical SST gradient than CA margin temperatures alone, which supports a causal link between long-term NAM strength and this temperature gradient. We next use isotope enabled simulations to corroborate this observed relationship between SST patterns, NAM strength, and δD_p .

NAM changes in Isotope-enabled Simulations

The iCAM5 experiment with Fu et al. (2022) SSTs produces a region of positive vapor δD anomalies that are co-located with warm SST anomalies. These vapor anomalies spatially coincide with the location of enriched δD_p and a weak, convergent, cyclonic circulation pattern (Figure 2). This is supported by the moisture budget analysis presented in Fu et al. (2022), which found that both thermodynamic and dynamic processes contributed to rainfall changes in their simulations. Because SST anomalies in the PRISM3 dataset are muted south of Baja California, δD_p is slightly depleted in that region, differing from our record from site 475 (Figure 2, Figure S5). However, this simulation still illustrates the connection between SST, vapor and precipitation δD , and summer rainfall.

In iCAM5, water vapor and precipitation δD act as tracers of changes in energy for convection. We measure the latter using equivalent potential temperature or θ_e , a thermodynamic quantity that integrates information about the temperature and moisture content of air parcels. Vertical gradients of θ_e therefore measure the potential for instability and convection. The vertical profile of the atmosphere over the NAM region shows that positive θ_e anomalies, which imply greater potential for convection, are co-located with increases in water vapor δD (Figure 2). Warmer subtropical SSTs likely drive higher local fluxes of sensible and latent heat. In addition, the convergent circulation over these warm coastal SSTs imports moist, warm air into this region (Fu et al., 2022). However, wind changes are small in this simulation. These

processes result in positive anomalies of θ_e , and also change the signature of δD_p by altering the isotopic signature of the moisture source from which precipitation is derived. Water vapor changes may dominate the isotopic response in iCAM5 because isotope-enabled models are known to underestimate δD_p changes that result directly from changing proportions of convective rainfall (Hu et al., 2018). Therefore, the model produces a smaller magnitude of change in δD_p compared to what is estimated by the proxies, although the model does overlap the 95% confidence interval of proxy-estimated δD_p change in the Pliocene at both sites.

Our iCAM5 simulation confirms that a stronger summer monsoon is linked to enriched δD_p and that warm temperatures along the California margin are critical for sustaining a stronger monsoon circulation. It is notable that the simulation produces an intensification of the NAM in both the core monsoon domain, as well as an expansion of the monsoon to the north and west (Figure 2), consistent with our interpretation that our leaf wax signals reflect hydroclimate changes associated with the NAM. However, this single simulation does not allow us to cleanly determine whether local warming on the CA margin, versus the gradient of temperature between the subtropical eastern Pacific and the EEP, is more important for driving an increase in summer rain. Furthermore, it is unclear whether intensification of the NAM alone could have sustained a positive balance of precipitation minus evaporation, as is implied by qualitative proxies like mesic vegetation, high lake levels, and taxa like Crocodylus.

To identify whether local CA margin SSTs or the larger subtropical/tropical SST gradient was responsible for the observed hydroclimatic changes, we conducted a series of simulations with iCAM5 where we systematically varied SST patterns (Figure S5). Across all of the simulations, annual P-E is strongly correlated with summer P-E (r = 0.87, p=0.04), which confirms that summer precipitation is important for maintaining a year-round positive P-E balance. However, we find a weak relationship between summer P-E and temperature anomalies on the southern CA margin (Figure 3a). Even when the model SST field overlaps the range of Pliocene proxy-inferred SST warming on the southern CA margin, the model does not produce positive P-E, as is implied by available qualitative proxies from the Pliocene. In contrast, summer P-E shows a statistically significant relationship with the subtropical/tropical SST gradient (Figure 3b). Simulations that weaken this gradient to near 2°C, which is within the range of the change suggested by Pliocene proxies, produce positive annual P-E that is primarily driven by changes in summer P-E (Figure 3b). While it is possible that the model underestimates the response of P-E to SST gradients since its low resolution does not resolve realistic patterns of moist convection, these simulations provide another line of evidence suggesting that NAM strength is determined by large-scale SST gradients between the tropics and subtropics, supporting the analyses of Pascale et al. (2017) and our hydroclimate and SST proxy data.

Implications for Current and Future Southwestern Hydroclimate

388

389

390

391

392

393

394

395

396

397

398

399

400

401

403

404

405

406

407

408

409

410

411

412

413

414

415

417

418

419

420

421

422

423

Pliocene proxy evidence and model simulations underscore the strong relationship between subtropical/tropical SST gradients in the east Pacific and NAM strength, with implications for understanding past and future climate in this region. Given the critical importance of temperature patterns to NAM variability, climate models with significant northeast Pacific SST bias may not produce reliable future predictions (Y. Zhu et al., 2020). This may contribute to a lack of robust predictions of future changes in the NAM, which tend to be highly dependent on model bias and resolution (Maloney et al., 2014; Meyer & Jin, 2017; Cook & Seager, 2013; Almazroui et al., 2021; Moon & Ha, 2020). When global SSTs are bias-corrected, high-resolution models produce robust decreases in rainfall across all seasons in response to warming (Pascale et al., 2017, 2018), at odds with previous work (Meyer & Jin, 2017; Cook & Seager, 2013). This result is due in part to reduced California margin warming compared to the tropical eastern Pacific (Pascale et al., 2017; He et al., 2020). In contrast, our results suggest that the Pliocene featured enhanced California margin warming compared to the tropical eastern Pacific, amplifying monsoon strength. This enhanced warming in Pliocene simulations may reflect the long-term influence of Earth system processes related to the cryosphere and vegetation, or long-term adjustments of deep ocean dynamics that alter SST patterns (Tierney et al., 2019; Feng et al., 2020; Brennan et al., 2022; A. Fedorov et al., 2013; Ford et al., 2015). In fact, a growing body of literature suggests that the equilibrium response of SST and hydroclimate to greenhouse boundary conditions, especially those that involve long-term Earth system feedbacks as likely occurred during the Pliocene, may differ fundamentally from responses to transient warming (Sniderman et al., 2019; Zappa et al., 2020; Burls & Fedorov, 2017; Feng et al., 2022).

Moreover, we are able to identify events in the observational record with amplified monsoon rainfall that parallel the mechanism of monsoon intensification in the Pliocene. Since the mid-20th century, the northeast Pacific has experienced multi-season or multi-year marine heat waves (MHW) (Myers et al., 2018; Amaya et al., 2020; Hoegh-Guldberg et al., 2014). The peak of a heat wave between 2012 and 2014 occurred in summer 2014 and featured SSTs 1- 2° C warmer than average on the southern California Margin (Myers et al., 2018), in a similar location to where proxies suggest the warmest mid-Pliocene temperatures occurred (Figure 4). During this event, eastern equatorial Pacific warming associated with a developing El Niño was muted. SST anomalies off the coast of Baja reached their maximum in summer 2014 (Myers et al., 2018). We use reanalysis data from the North American Regional Reanalysis (NARR) and the NCEP-NCAR reanalysis (Mesinger et al., 2006; Kalnay et al., 1996) to plot changes in precipitation, winds, and calculate changes in equivalent potential temperature θ_e . To quantify changes in deep convection, we plot changes in summertime (June - September)

climatological outgoing longwave radiation (OLR) over southern Baja California as well as the distribution of OLR values during the heat wave (Liebmann & Smith, 1996). Lower values of OLR indicate cooler cloud tops and deeper convection (Figure 4).

424

425

426

427

428

429

430

431

432

433

434

435

436

437

439

440

441

442

443

444

445

446

447

448

449

450

451

453

454

455

456

Statistically significant rainfall changes occur in the core NAM domain, but also in peripheral regions like the Baja California Peninsula, which normally experiences atmospheric subsidence and receives little monsoon rain (Figure S6) (Fonseca-Hernandez et al., 2021). This is illustrated by a shift in daily summertime outgoing longwave radiation (OLR) over Baja, which shows an increase to near 240–250 W/m². These values are characteristic of monsoon storms, while outlying low values represent tropical storms and hurricanes (Figure 4). This increased convection is partially the result of the direct thermodynamic effect of warm SSTs, but we also note the presence of stronger southerly winds along the coast of Mexico (Figure 4). Circulation changes and warm SSTs increase low level moist entropy, enhancing moist convection over the NAM region (Figure 4). Our results are further corroborated by previous research showing that extreme rainfall and flooding in southern Arizona is linked to increased precipitable water offshore of Baja, similar to what we observe during the MHW (Yang et al., 2017). Moreover, previous work found that other NE Pacific marine heat waves are associated with above average soil moisture across the NAM domain (Shi et al., 2021).

Disentangling causality in a short instrumental record is challenging, and the cause of MHW-related SST anomalies, which result from changes in surface radiation, may differ from the cause of the California margin warming in the Pliocene, which could also involve ocean dynamical adjustments (Myers et al., 2018; Brennan et al., 2022; Ford et al., 2015; A. Fedorov et al., 2013). Despite this, there are clear parallels between our conceptual model of Pliocene NAM changes and MHW-related NAM changes. For reference, we plot the 2014 marine heat wave on Figure 3. This event stands out as featuring only modest California margin SST anomalies, far below the range of those inferred by Pliocene proxies. However, because this marine heat wave event was paired with weak positive temperature anomalies in the EEP, this event featured a greatly relaxed subtropical/tropical SST gradient. This example suggests that, if MHW similar to those observed in 2013-2014 continue to intensify as projected, the future may feature intervals with SST patterns and circulation anomalies that are conducive to more intense, spatially expanded NAM rainfall. These extreme events in turn have important societal and ecological consequences, including potentially amplifying wildfire risk by increasing plant biomass and fuel loads, and increasing hazards from landslides associated with extreme rainfall events (Mazon et al., 2016; Demaria et al., 2019; Pascale et al., 2018).

Conclusions

Two novel leaf wax reconstructions of SWNA hydroclimate provide proxy evidence of intensification of the NAM, as well as expansion of its spatial footprint, during the Pliocene. Instead of solely resulting from winter rain changes, wet conditions during this epoch were at least in part driven by the summer monsoon. In fact, model simulations suggest that the majority of the precipitation minus evaporation signal in the Pliocene may have been driven by summer rainfall. Both proxies and models suggest that the Pliocene expansion of summer rainfall in SWNA is linked to the subtropical/tropical SST gradient across the eastern Pacific. These results cohere with the model experiments in Pascale et al. (2017), who posit that this gradient will play a key role in the future trajectory of the NAM. Our results are also consistent with the 'warmer-get-wetter' paradigm, which posits that, in warm climates, the largest rainfall changes in the subtropics and tropics should occur in regions with the highest *relative* SST warming (Xie et al., 2010). They also cohere with previous work that speculated about a linkage between eastern Pacific SSTs, atmospheric stability and NAM convection in past and future climate states (Bakun, 1990; Barron et al., 2012).

SWNA is in the midst of an intensifying megadrought, driven in part by higher temperatures that increase evaporation and reduce snowpack (Williams et al., 2022). Understanding the role of monsoon rainfall in future hydroclimate has implications for regional water resources, ecosystems, wildfire regimes, and other land surface processes. There is currently no consensus about the future trajectory of the monsoon. However, recent simulations suggest that the future will feature a weaker NAM, as a result of a reduced eastern Pacific subtropical/tropical gradient that enhances atmospheric stability over SWNA (Pascale et al., 2017). This is the opposite of what proxies suggest for the Pliocene, which featured a greatly reduced reduced subtropical/tropical gradient (Brierley et al., 2009a; A. V. Fedorov et al., 2015). One possible reason for this discrepancy is because of the timescale of response for the Pliocene vs. near-future warming: the Pliocene represents an equilibrium climate state and features SST patterns that are the result of long-term adjustments of the Earth system that have yet to emerge in transient simulations of current warming (Heede et al., 2021; Rugenstein et al., 2020).

Our analysis of the observational record also suggests that the future may be characterized by intervals of expanded monsoon rainfall. We demonstrated that marine heat waves on the southern California Margin, when coupled with muted warming in the EEP, result in a stronger monsoon. While the direct influence of CO₂ is predicted to intensify individual monsoon storms (Demaria et al., 2019; Pascale et al., 2018), marine heat waves complement this mechanism by facilitating the spatial expansion of monsoon rainfall into regions like Baja and southern California. This example raises the intriguing possibility that the subtropical/tropical SST gradient may help aid efforts to improve the seasonal predictability of NAM rainfall (Grimm et

al., 2020). In models, future shifts in the strength and position of the North Pacific subtropical high are likely to weaken upwelling-favorable winds along the California margin, creating changes in mean temperatures and potentially altering the frequency of local marine heat waves (Schmidt et al., 2020; Rykaczewski et al., 2015). However, current generation models are known to underestimate the intensity and duration of marine heat waves (Plecha & Soares, 2020), suggesting that alternate model configurations, possibly featuring higher oceanic resolution, may be key to estimating future changes in California margin marine heat waves and their impact on monsoon rainfall. Clarifying the future behavior of this mechanism will have important implications for our understanding of landscape and water management, since periods of enhanced summer rain coupled to a warmer climate may result in higher fuel loads and fire, as well as flash flooding (Moloney et al., 2019; Yang et al., 2017).

Our results have implications for both past and future hydroclimate change in SWNA. Several modeling studies have shown that subtropical regions, especially eastern ocean boundary upwelling zones, are especially sensitive to greenhouse boundary conditions (Schneider et al., 2019; J. Zhu et al., 2019). It is therefore likely that other greenhouse climate intervals witnessed similar hydroclimate reorganizations on land areas near upwelling zones. The mechanism we identify is also relevant to the present day, since we found evidence of an expanded monsoon during the modern 2014 marine heat wave. These results underscore the fact that far from representing a climate state fundamentally dissimilar from present day, the Pliocene can both help test fundamental theories about the dynamics that govern regional circulation, and serve as an analog for the processes that will drive hydroclimate in a warmer world. Further studies of the Pliocene and similar greenhouse intervals could therefore provide key lessons relevant for adapting to both near-future and long-term regional hydroclimate changes.

Data Availability Statement

Newly generated datasets from DSDP 475 and ODP 1012 are available on the NOAA/NCEI Paleoclimatology Database at Bhattacharya et al. (2022b). New isotope-enable simulations with iCAM5 have also been archived in public repositories. Consistent with Fu et al. (2022), iCAM5 simulations using fixed SSTs from that paper have been archived at the Open Science Framework (OSF) and can be found at Bhattacharya et al. (2022c). iCAM5 simulations associated with the fixed SST sensitivity experiments in this paper are available in Zenodo and can be found at Bhattacharya et al. (2022a). The North American Regional Reanalysis can be accessed at https://www.ncei.noaa.gov/products/weather-climate-models/north-american-regional. Model code for isotope-enabled CESM can be obtained at https://github.com/NCAR/iCESM1.2.

Conflict of Interest

The authors declare no conflicts of interest relevant to this study.

Acknowledgments

TB acknowledges funding support from NSF Grants Paleo Perspectives on Climate Change (P2C2) OCE-1903148 and OCE-2103015. Measurements were made possible with support from NSF MRI Grant EAR-2018078 to TB. MF was supported by the NSF Climate Dynamics program (joint NSF/NERC) grant AGS-1924538. JET acknowledges funding support from NSF OCE-1651034 and OCE-1903171. NJB and SK acknowledge funding support from NSF award AGS-1844380. RF acknowledges funding from NSF Grants OCE-2103055 and OCE-1903650. All simulations were conducted on Computational and Information Systems Laboratory. 2019. Cheyenne: HPE/SGI ICE XA System (Climate Simulation Laboratory). Boulder, CO: National Center for Atmospheric Research. doi:10.5065/D6RX99HX. We thank lab managers Patrick Murphy at the University of Arizona and Jillian Aluisio and Stephanie Bullinger at Syracuse University for assistance with the leaf wax analysis, and Debbie Colodner, Amy Orchard, and the Junior Docents from The Arizona-Sonora Desert Museum for assisting with the collection of modern desert plants.

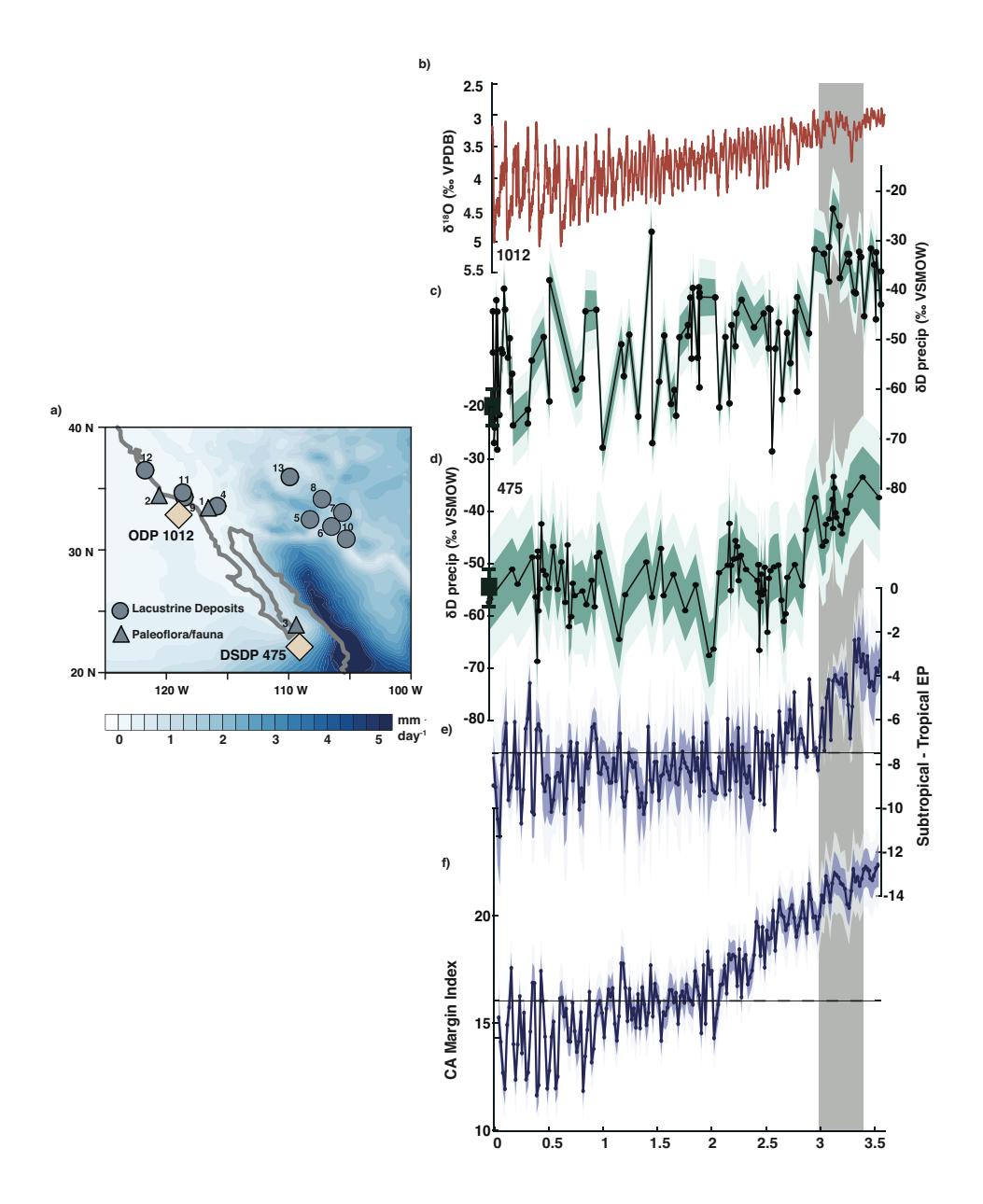


Figure 1. Plio-Pleistocene changes in SWNA hydroclimate. a) Climatological summertime precipitation across the SWNA (Mesinger et al., 2006), the locations of qualitative proxies indicating wetter conditions during the Pliocene (see Table S1), and the locations of the cores investigated in this study (ODP 1012 and DSDP 475). b) Benthic oxygen isotope stack from (Lisiecki & Raymo, 2005). c) and d) New Plio-Pleistocene reconstructions of δD_p from ODP 1012 and DSDP 475 respectively. Modern coretop values are shown as dark green squares with 1σ -error bars. e) Index of subtropical minus tropical eastern Pacific sea-surface temperature. f) Index of Plio-Pleistocene CA margin sea-surface temperature.

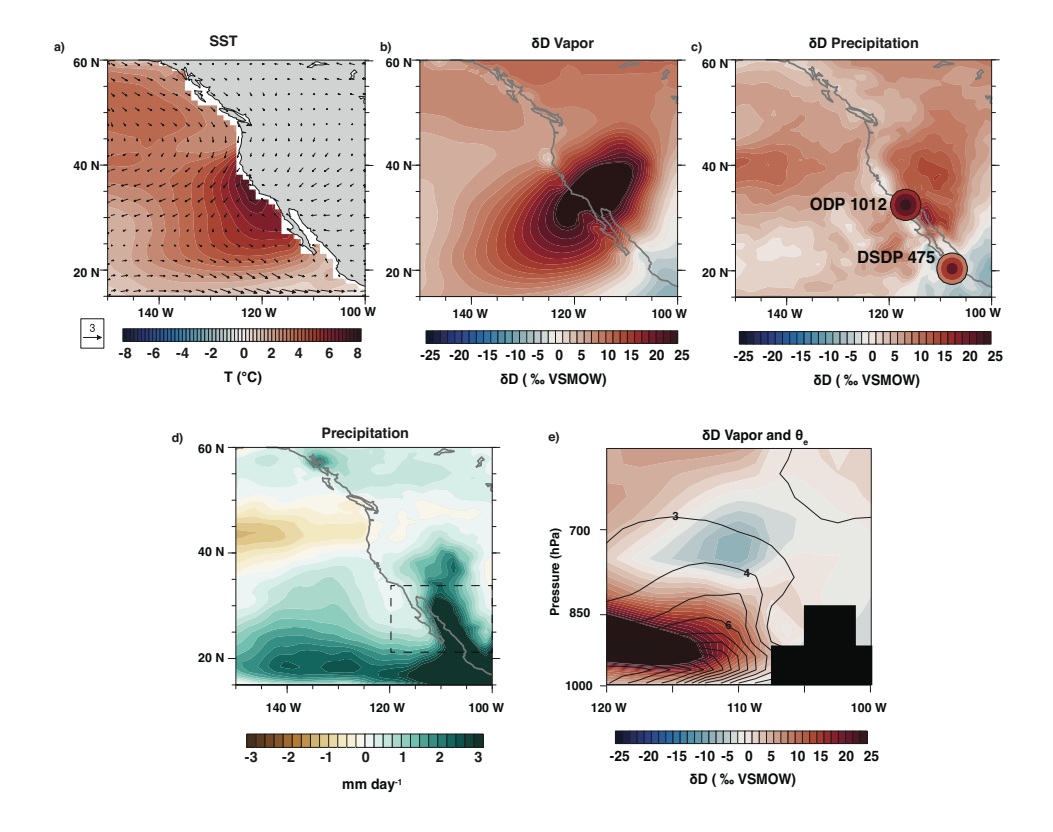


Figure 2. Summer rainfall and water isotopes in an isotope-enabled simulation forced with idealized SST changes (Fu et al., 2022). a) June-September SST and 850 mb wind anomalies. b) Vertically integrated δD of water vapor anomalies. c) δD_p anomalies, with lower (outer circle), median (middle circle), and upper (inner circle) 95% confidence interval of proxy-estimated δD_p changes at site 475 and 1012. d) Precipitation anomalies. e) The vertical profile of lower-atmospheric changes in δD of vapor and θ_e in the dashed box shown in panel d). Black outline masks areas that are below the land surface in this model.

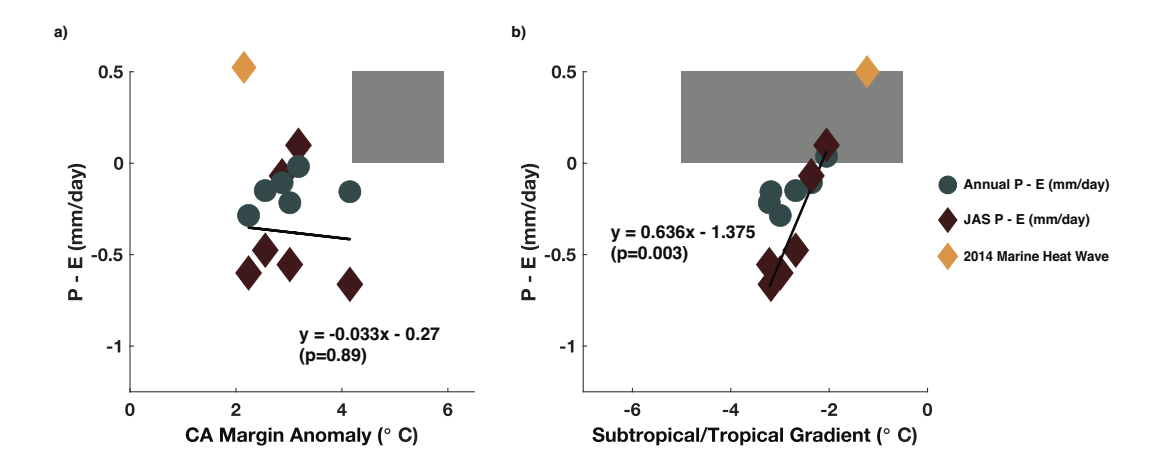


Figure 3. Relationship between SST patterns and SWNA hydroclimate in iCAM5 simulations. Red diamonds indicate changes in summer precipitation minus evaporation (P-E, mm/day); blue-green circles indicate annual P-E. a) The relationship between southern CA margin SST anomalies (SST changes between 20-35°N and 125-110°W) and P-E across SWNA (land areas between 20-35°N and 120-105°W). Gray box shows 95% confidence interval of proxy-inferred southern CA margin warming, and is located above 0 P-E since qualitative proxies (lake level, flora/fauna) suggest positive anomalies of P-E during the Pliocene. b) the relationship between the subtropical/tropical gradient and P-E. The SST gradient is calculated by taking the CA margin SST anomalies in a) and subtracting EEP temperatures (averaged between 5°S - 5°N and 170-90°W). Gray box shows proxy-inferred range of this gradient. For reference, SST and summertime P-E anomalies for the 2014 marine heat wave results presented in Figure 4 are shown as yellow diamonds.

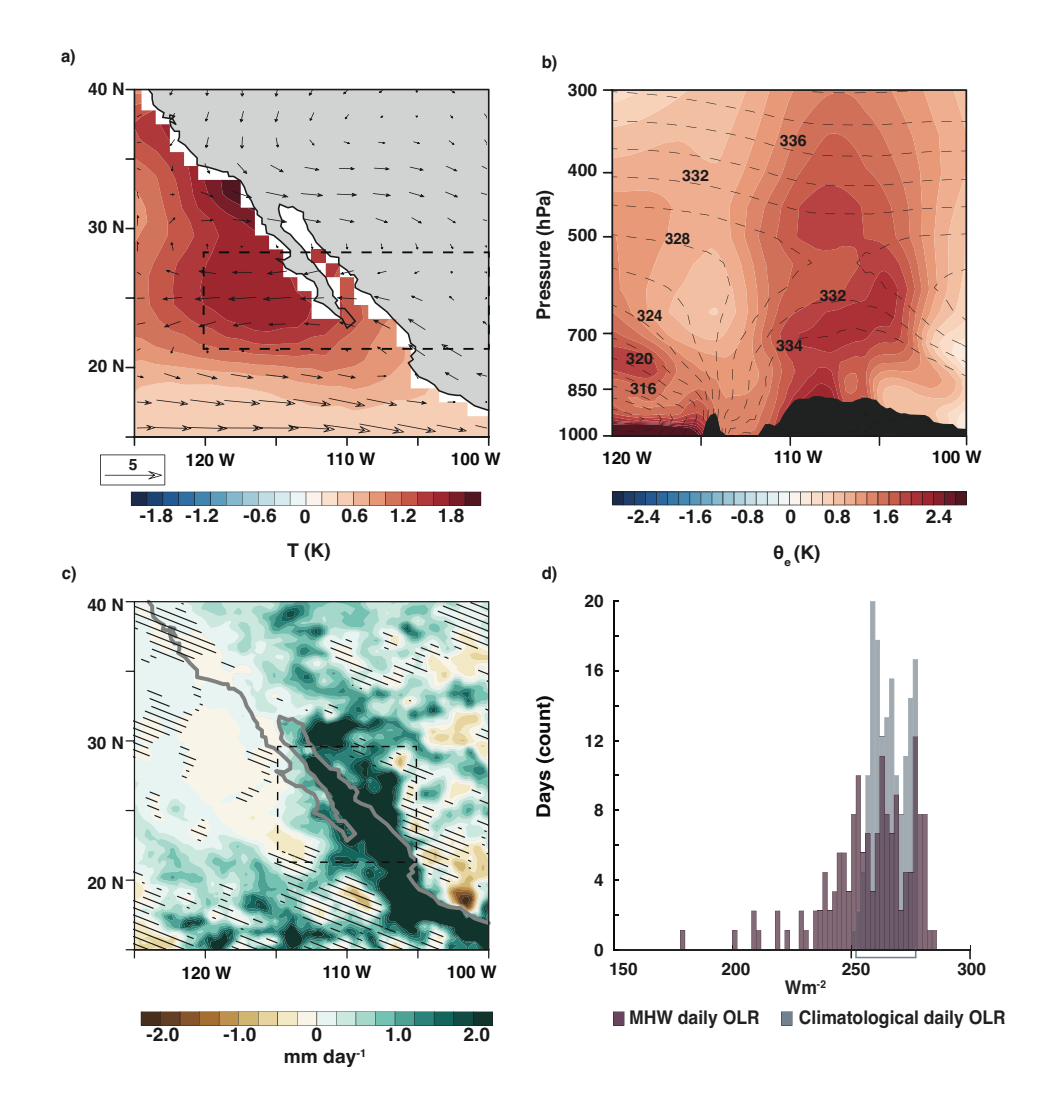


Figure 4. NAM changes during the peak of the 2014 northeast Pacific MHW. a) SST anomalies during summer 2014, the peak of the MHW, with dashed box showing location of vertical profile in panel b). b) Vertical atmospheric profile of moist entropy (θ_e) changes over Baja California in box shown in panel c). Dashed contours show climatological values, while colored contours indicate 2014 MHW anomalies. c) Rainfall anomalies in the North American Regional Analysis, with stippling showing values that are not significant at the 95% level. d) The daily distribution of climatological (gray) and MHW (purple) summertime outgoing longwave radiation (OLR). Lower OLR values indicate cooler cloud tops on deep convective clouds. Gray bracket shows 95% CI for climatological values.

References

543

- Aggarwal, P. K., Romatschke, U., Araguas-Araguas, L., Belachew, D., Longstaffe, F. J.,
- Berg, P., ... Funk, A. (2016). Proportions of convective and stratiform precipitation revealed in water isotope ratios. *Nature Geoscience*, *9*(8), 624–629.
- Almazroui, M., Islam, M. N., Saeed, F., Saeed, S., Ismail, M., Ehsan, M. A., ... others
- 548 (2021). Projected changes in temperature and precipitation over the United States,
- Central America, and the Caribbean in CMIP6 GCMs. *Earth Systems and Environ- ment*, *5*(1), 1–24.
- Amaya, D. J., Miller, A. J., Xie, S.-P., & Kosaka, Y. (2020). Physical drivers of the summer 2019 North Pacific marine heatwave. *Nature communications*, *11*(1), 1–9.
- Axelrod, D. I. (1948). Climate and evolution in western North America during middle Pliocene time. *Evolution*, 127–144.
- Bakun, A. (1990). Global climate change and intensification of coastal ocean upwelling. *Science*, 247(4939), 198–201.
- Ballog, R. A., & Malloy, R. E. (1981). Neogene Palynology from the Southern California Continental Borderland, Site 467, Deep Sea Drilling Project Leg 64 (Vol. 63). U.S. Government Printing Office.
- Barron, J. A., Metcalfe, S. E., & Addison, J. A. (2012). Response of the North American monsoon to regional changes in ocean surface temperature. *Paleoceanography*, 27(3).
- Bhattacharya, T., Feng, R., Tierney, J., Rubbelke, N., C. and Burls, Knapp, S., & Fu, M.
- 563 (2022a). Expansion and intensification of the north american monsoon during the
 564 pliocene[dataset]. Zenodo. Retrieved from https://doi.org/10.5281/
 565 zenodo.7036092
- Bhattacharya, T., Feng, R., Tierney, J., Rubbelke, N., C .and Burls, Knapp, S., & Fu, M.
- 567 (2022b). Hydrogen isotopic reconstruction of north american monsoon since
 568 mid-pliocene [dataset]. NOAA/NCEI Paleocimatology Database. Retrieved from
 569 https://www.ncei.noaa.gov/access/paleo-search/study/36778
- Bhattacharya, T., Feng, R., Tierney, J., Rubbelke, N., C .and Burls, Knapp, S., & Fu, M.
- 571 (2022c). Isotope enabled simulations for expansion and intensification of the north
 572 american monsoon during the pliocene [dataset]. *Open Science Framework*. Retrieved
 573 from https://doi.org/10.17605/OSF.IO/REWJ5
- Bhattacharya, T., Tierney, J. E., Addison, J. A., & Murray, J. W. (2018). Ice-sheet modulation of deglacial North American monsoon intensification. *Nature Geoscience*, *11*(11), 848–852.
- Brady, E., Stevenson, S., Bailey, D., Liu, Z., Noone, D., Nusbaumer, J., ... others (2019).

 The connected isotopic water cycle in the Community Earth System Model version 1.
- Journal of Advances in Modeling Earth Systems, 11(8), 2547–2566.

- Brennan, P. R., Bhattacharya, T., Feng, R., Tierney, J. E., & Jorgensen, E. (2022). Patterns and mechanisms of northeast pacific temperature response to pliocene boundary conditions. *Paleoceanography and Paleoclimatology*, *37*(7), e2021PA004370.
- Brierley, C. M., Fedorov, A. V., Liu, Z., Herbert, T. D., Lawrence, K. T., & LaRiviere, J. P. (2009a). Greatly expanded tropical warm pool and weakened Hadley circulation in the early Pliocene. *Science*, *323*(5922), 1714–1718.
- Brierley, C. M., Fedorov, A. V., Liu, Z., Herbert, T. D., Lawrence, K. T., & LaRiviere, J. P.

 (2009b, March). Greatly Expanded Tropical Warm Pool and Weakened Hadley Circulation in the Early Pliocene. *Science*, 323(5922), 1714–1718. Retrieved 2021-05-02, from https://science.sciencemag.org/content/323/5922/1714

 (Publisher: American Association for the Advancement of Science Section: Report)

 doi: 10.1126/science.1167625
- Burls, N. J., & Fedorov, A. V. (2017). Wetter subtropics in a warmer world: Contrasting past and future hydrological cycles. *Proceedings of the National Academy of Sciences*, 114(49), 12888–12893.
- Byrne, M. P., & O'Gorman, P. A. (2015). The response of precipitation minus evapotranspiration to climate warming: Why the "wet-get-wetter, dry-get-drier" scaling does not hold over land. *Journal of Climate*, 28(20), 8078–8092.
- Collister, J. W., Rieley, G., Stern, B., Eglinton, G., & Fry, B. (1994). Compound-specific δ 13C analyses of leaf lipids from plants with differing carbon dioxide metabolisms. *Organic geochemistry*, 21(6-7), 619-627.
- Cook, B. I., & Seager, R. (2013). The response of the North American Monsoon to increased greenhouse gas forcing. *Journal of Geophysical Research: Atmospheres*, 118(4), 1690–1699.
- Curray, J., Moore, D., Aguayo, J., Aubry, M.-P., Einsele, G., Fornari, D., ... Vacquier,

 V. (1982). Baja California Passive Margin Transect: Sites 474, 475, and 476

 (Vol. 64). U.S. Government Printing Office. Retrieved 2021-04-06, from http://deepseadrilling.org/64/dsdp_toc.htm doi: 10.2973/dsdp.proc.64.1982

(2007).

Warm upwelling

regions in the Pliocene warm period. Paleoceanography, 22(3). Retrieved 2021-04-06, from http://agupubs.onlinelibrary

wiley.com/doi/abs/10.1029/2006PA001394 (_eprint:
https://onlinelibrary.wiley.com/doi/pdf/10.1029/2006PA001394) doi: https://doi.org/
10.1029/2006PA001394

Dekens, P. S., Ravelo, A. C., & McCarthy, M. D.

608

Demaria, E. M., Hazenberg, P., Scott, R. L., Meles, M. B., Nichols, M., & Goodrich, D.

(2019). Intensification of the North American Monsoon rainfall as observed from
a long-term high-density gauge network. *Geophysical Research Letters*, 46(12),

- 6839–6847.
- Douglas, M. W., & Leal, J. C. (2003). Summertime surges over the Gulf of California:
- Aspects of their climatology, mean structure, and evolution from radiosonde, NCEP
- reanalysis, and rainfall data. Weather and forecasting, 18(1), 55–74.
- Dowsett, H., Robinson, M., & Foley, K. (2009). Pliocene three-dimensional global ocean temperature reconstruction. *Climate of the Past*, *5*(4), 769–783.
- Durazo, R., & Baumgartner, T. (2002). Evolution of oceanographic conditions off Baja California: 1997–1999. *Progress in Oceanography*, *54*(1-4), 7–31.
- Etourneau, J., Schneider, R., Blanz, T., & Martinez, P. (2010, August). Intensification of the Walker and Hadley atmospheric circulations during the Pliocene–Pleistocene climate
- transition. Earth and Planetary Science Letters, 297(1), 103-110. Retrieved 2021-05-
- 02, from https://www.sciencedirect.com/science/article/pii/
- 50012821X10003845 doi: 10.1016/j.epsl.2010.06.010
- Fedorov, A., Brierley, C., Lawrence, K. T., Liu, Z., Dekens, P., & Ravelo, A. (2013). Patterns and mechanisms of early Pliocene warmth. *Nature*, 496(7443), 43–49.
- Fedorov, A. V., Burls, N. J., Lawrence, K. T., & Peterson, L. C. (2015). Tightly linked zonal and meridional sea surface temperature gradients over the past five million years. *Nature Geoscience*, 8(12), 975–980.
- Feng, R., Bhattacharya, T., Otto-Bliesner, B. L., Brady, E. C., Haywood, A. M., Tindall,
 J. C., ... others (2022). Past terrestrial hydroclimate sensitivity controlled by earth
 system feedbacks. *Nature Communications*, *13*(1), 1–11.
- Feng, R., Otto-Bliesner, B. L., Brady, E. C., & Rosenbloom, N. (2020). Increased climate response and earth system sensitivity from CCSM4 to CESM2 in mid-Pliocene simulations. *Journal of Advances in Modeling Earth Systems*, *12*(8), e2019MS002033.
- Fonseca-Hernandez, M., Turrent, C., Mayor, Y. G., & Tereshchenko, I. (2021). Using observational and reanalysis data to explore the southern Gulf of California boundary layer during the North American Monsoon onset. *Journal of Geophysical Research:*Atmospheres, 126(7), e2020JD033508.
- Ford, H. L., Ravelo, A. C., Dekens, P. S., LaRiviere, J. P., & Wara, M. W. (2015). The evolution of the equatorial thermocline and the early Pliocene El Padre mean state. *Geo-physical Research Letters*, 42(12), 4878–4887.
- Fu, M., Cane, M. A., Molnar, P., & Tziperman, E. (2022, January). Warmer Pliocene upwelling site SST leads to wetter subtropical coastal areas: a positive feedback on SST. *Paleoceanography and Paleoclimatology*, e2021PA004357.
- Gao, L., Edwards, E. J., Zeng, Y., & Huang, Y. (2014). Major evolutionary trends in hydrogen isotope fractionation of vascular plant leaf waxes. *PloS one*, *9*(11), e112610.
- 653 Grimm, A. M., Dominguez, F., Cavalcanti, I. F., Cavazos, T., Gan, M. A., Silva Dias, P. L.,

- 654 ... Barreiro, M. (2020). South and North American Monsoons: Characteristics, life 655 cycle, variability, modeling, and prediction. In *The multiscale global monsoon system* 656 (pp. 49–66). World Scientific.
- He, C., Li, T., & Zhou, W. (2020). Drier North American monsoon in contrast to Asian– African monsoon under global warming. *Journal of Climate*, *33*(22), 9801–9816.
- Heede, U. K., Fedorov, A. V., & Burls, N. J. (2021). A stronger versus weaker Walker: understanding model differences in fast and slow tropical Pacific responses to global warming. *Climate Dynamics*, *57*(9), 2505–2522.
- Herbert, T., Schuffert, J., Andreasen, D., Heusser, L., Lyle, M., Mix, A., ... Herguera, J.

 (2001). Collapse of the california current during glacial maxima linked to climate change on land. *Science*, 293(5527), 71–76.
- Herbert, T. D., Lawrence, K. T., Tzanova, A., Peterson, L. C., Caballero-Gill, R., & Kelly,

 C. S. (2016, November). Late Miocene global cooling and the rise of modern

 ecosystems. Nature Geoscience, 9(11), 843–847. Retrieved 2021-05-02, from

 https://www.nature.com/articles/ngeo2813 (Number: 11 Publisher:

 Nature Publishing Group) doi: 10.1038/ngeo2813
- Higgins, R., Mo, K., & Yao, Y. (1998). Interannual variability of the US summer precipitation regime with emphasis on the southwestern monsoon. *Journal of Climate*, *11*(10), 2582–2606.
- Hoegh-Guldberg, O., Cai, R., Poloczanska, E., Brewer, P., Sundby, S., Hilmi, K., . . . Jung,

 S. (2014). The ocean. in: Climate change 2014: Impacts, adaptation, and vulnerability. part b: Regional aspects. contribution of working group ii to the fifth assessment
 report of the intergovernmental panel on climate change. Intergovernmental Panel on
 Climate Change.
- Hu, J., Emile-Geay, J., Nusbaumer, J., & Noone, D. (2018). Impact of convective activity on precipitation δ 180 in isotope-enabled general circulation models. *Journal of Geophysical Research: Atmospheres*, 123(23), 13–595.
- Ibarra, D. E., Oster, J. L., Winnick, M. J., Caves Rugenstein, J. K., Byrne, M. P., & Chamber-lain, C. P. (2018). Warm and cold wet states in the western United States during the Pliocene–Pleistocene. *Geology*, 46(4), 355–358.
- Kalnay, E., Kanamitsu, M., Kistler, R., Collins, W., Deaven, D., Gandin, L., . . . Joseph, D.

 (1996). The ncep/ncar 40-year reanalysis project. *Bulletin of the American meteoro-logical Society*, 77(3), 437–472.
- LaRiviere, J. (2007). California margin sea surface temperature and paleoproductivity

 records at ocean drilling program site 1012. Southern Illinois University at Carbondale.
- LaRiviere, J. P., Ravelo, A. C., Crimmins, A., Dekens, P. S., Ford, H. L., Lyle, M., & Wara,

- M. W. (2012, June). Late Miocene decoupling of oceanic warmth and atmospheric carbon dioxide forcing. *Nature*, 486(7401), 97–100. Retrieved 2021-05-02, from https://www.nature.com/articles/nature11200 (Number: 7401)
- Publisher: Nature Publishing Group) doi: 10.1038/nature11200
- Lawrence, K. T., Liu, Z., & Herbert, T. D. (2006, April). Evolution of the Eastern Tropical Pacific Through Plio-Pleistocene Glaciation. *Science*, 312(5770), 79–83. Retrieved 2021-05-12, from https://science.sciencemag.org/content/312/
- 698 5770/79 (Publisher: American Association for the Advancement of Science Sec-699 tion: Research Article) doi: 10.1126/science.1120395
- Liebmann, B., & Smith, C. A. (1996). Description of a complete (interpolated) outgoing longwave radiation dataset. *Bulletin of the American Meteorological Society*, 77(6), 1275–1277.
- Lisiecki, L. E., & Raymo, M. E. (2005). A Pliocene-Pleistocene stack of 57 globally distributed benthic $\delta 180$ records. *Paleoceanography*, 20(1).
- Liu, J., Tian, J., Liu, Z., Herbert, T. D., Fedorov, A. V., & Lyle, M. (2019, April). Eastern equatorial Pacific cold tongue evolution since the late Miocene linked to extratropical climate. *Science Advances*, *5*(4), eaau6060. Retrieved 2021-07-11, from
- https://advances.sciencemag.org/content/5/4/eaau6060 (Pub-
- lisher: American Association for the Advancement of Science Section: Research
 Article) doi: 10.1126/sciadv.aau6060
- Maloney, E. D., Camargo, S. J., Chang, E., Colle, B., Fu, R., Geil, K. L., ... others (2014).

 North American climate in CMIP5 experiments: Part III: Assessment of twenty-firstcentury projections. *Journal of Climate*, 27(6), 2230–2270.
- Mazon, J. J., Castro, C. L., Adams, D. K., Chang, H.-I., Carrillo, C. M., & Brost, J. J. (2016).
 Objective climatological analysis of extreme weather events in Arizona during the
 North American monsoon. *Journal of Applied Meteorology and Climatology*, 55(11),
 2431–2450.
- Mesinger, F., DiMego, G., Kalnay, E., Mitchell, K., Shafran, P. C., Ebisuzaki, W., ... Shi, W. (2006). North american regional reanalysis. *Bulletin of the American Meteorological Society*, 87(3), 343–360.
- Meyer, J. D., & Jin, J. (2017). The response of future projections of the North American monsoon when combining dynamical downscaling and bias correction of CCSM4 output. *Climate Dynamics*, *49*(1), 433–447.
- Miller, W. E. (1980). The late Pliocene Las Tunas local fauna from southernmost Baja California, Mexico. *Journal of Paleontology*, 762–805.
- Mix, H. T., Rugenstein, J. K. C., Reilly, S. P., Ritch, A. J., Winnick, M. J., Kukla, T., & Chamberlain, C. P. (2019). Atmospheric flow deflection in the late cenozoic sierra

- nevada. Earth and Planetary Science Letters, 518, 76–85.
- Molnar, P., & Cane, M. A. (2002). El Niño's tropical climate and teleconnections as a blueprint for pre-Ice Age climates. *Paleoceanography*, *17*(2), 11–1.
- Moloney, K. A., Mudrak, E. L., Fuentes-Ramirez, A., Parag, H., Schat, M., & Holzapfel, C. (2019). Increased fire risk in Mojave and Sonoran shrublands due to exotic species and extreme rainfall events. *Ecosphere*, *10*(2), e02592.
- Moon, S., & Ha, K.-J. (2020). Future changes in monsoon duration and precipitation using CMIP6. *npj Climate and Atmospheric Science*, *3*(1), 1–7.
- Myers, T. A., Mechoso, C. R., Cesana, G. V., DeFlorio, M. J., & Waliser, D. E. (2018).
 Cloud feedback key to marine heatwave off Baja California. *Geophysical Research* Letters, 45(9), 4345–4352.
- Nusbaumer, J., Wong, T. E., Bardeen, C., & Noone, D. (2017). Evaluating hydrological processes in the C ommunity A tmosphere M odel V ersion 5 (C AM5) using stable isotope ratios of water. *Journal of Advances in Modeling Earth Systems*, *9*(2), 949–977.
- Ostertag-Henning, C., & Stax, R. (2000). Data report: Carbonate records from sites 1012, 1013, 1017, and 1019 and alkenone-based sea-surface temperatures from site 1017. In *Proc. ocean drill. program, sci. results* (Vol. 167, pp. 297–302).
- Pascale, S., Boos, W. R., Bordoni, S., Delworth, T. L., Kapnick, S. B., Murakami, H., . . .
 Zhang, W. (2017). Weakening of the North American monsoon with global warming.
 Nature Climate Change, 7(11), 806–812.
- Pascale, S., Kapnick, S. B., Bordoni, S., & Delworth, T. L. (2018). The influence of CO2 forcing on North American monsoon moisture surges. *Journal of Climate*, *31*(19), 7949–7968.
- Plecha, S. M., & Soares, P. M. (2020). Global marine heatwave events using the new cmip6 multi-model ensemble: from shortcomings in present climate to future projections. *Environmental Research Letters*, *15*(12), 124058.
- Pound, M., Tindall, J., Pickering, S., Haywood, A., Dowsett, H., & Salzmann, U. (2014).

 Late Pliocene lakes and soils: a global data set for the analysis of climate feedbacks in
 a warmer world. *Climate of the Past*, 10(1), 167–180.
- Pound, M. J., Haywood, A. M., Salzmann, U., & Riding, J. B. (2012). Global vegetation dynamics and latitudinal temperature gradients during the mid to late miocene (15.97–5.33 ma). *Earth-Science Reviews*, 112(1-2), 1–22.
- Remeika, P., Fischbein, I. W., & Fischbein, S. A. (1988). Lower Pliocene petrified wood from the Palm Spring Formation, Anza Borrego Desert State Park, California. *Review of palaeobotany and palynology*, *56*(3-4), 183–198.
- Rousselle, G., Beltran, C., Sicre, M.-A., Raffi, I., & De Rafélis, M. (2013, January).

- Changes in sea-surface conditions in the Equatorial Pacific during the middle 765
- Miocene–Pliocene as inferred from coccolith geochemistry. Earth and Plane-766
- Retrieved 2021-05-02, from https://www tary Science Letters, 361, 412-421. 767
- .sciencedirect.com/science/article/pii/S0012821X12006115 768
- doi: 10.1016/j.epsl.2012.11.003
- Rugenstein, M., Bloch-Johnson, J., Gregory, J., Andrews, T., Mauritsen, T., Li, C., ... 770
- Knutti, R. (2020).Equilibrium climate sensitivity estimated by equilibrating cli-771 mate models. Geophysical Research Letters, 47(4), e2019GL083898.
- Rykaczewski, R. R., Dunne, J. P., Sydeman, W. J., García-Reyes, M., Black, B. A., & Bo-
- grad, S. J. Poleward displacement of coastal upwelling-favorable winds in (2015).774
- the ocean's eastern boundary currents through the 21st century. Geophysical Research 775
- Letters, 42(15), 6424-6431. 776

772

- Sachse, D., Billault, I., Bowen, G. J., Chikaraishi, Y., Dawson, T. E., Feakins, S. J., ... oth-777
- ers (2012). Molecular paleohydrology: interpreting the hydrogen-isotopic composition 778
- of lipid biomarkers from photosynthesizing organisms. Annual Review of Earth and
- Planetary Sciences, 40, 221-249. 780
- 781 Salzmann, U., Haywood, A. M., & Lunt, D. J. (2009).The past is a guide to the future?
- Comparing Middle Pliocene vegetation with predicted biome distributions for the 782
- twenty-first century. Philosophical Transactions of the Royal Society A: Mathematical, 783
- Physical and Engineering Sciences, 367(1886), 189–204. 784
- Schmidt, D. F., Amaya, D. J., Grise, K. M., & Miller, A. J. (2020). Impacts of shifting sub-785
- tropical highs on the California Current and Canary Current systems. Geophysical Re-786
- search Letters, 47(15), e2020GL088996. 787
- Schneider, T., Kaul, C. M., & Pressel, K. G. (2019).Possible climate transitions from 788
- breakup of stratocumulus decks under greenhouse warming. Nature Geoscience, 789
- *12*(3), 163–167.
- Schrag, D. P., Hampt, G., & Murray, D. W. (1996). Pore fluid constraints on the tempera-791
- ture and oxygen isotopic composition of the glacial ocean. Science, 272(5270), 1930-792
- 1932. 793
- Schumacher, C., & Houze, R. A. (2003). The TRMM precipitation radar's view of shallow,
- isolated rain. Journal of Applied Meteorology and Climatology, 42(10), 1519-1524. 795
- Seager, R., Naik, N., & Vecchi, G. A. (2010). Thermodynamic and dynamic mechanisms 796
- for large-scale changes in the hydrological cycle in response to global warming. Jour-797
- nal of climate, 23(17), 4651-4668. 798
- Seki, O., Schmidt, D. N., Schouten, S., Hopmans, E. C., Damsté, J. S. S., & Pancost, R. D. 799
- Paleoceanographic changes in the Eastern Equatorial Pacific over the last 10 (2012).800
- Myr. Paleoceanography, 27(3). Retrieved 2021-05-02, from https://agupubs 801

- .onlinelibrary.wiley.com/doi/abs/10.1029/2011PA002158 802
- (_eprint: https://agupubs.onlinelibrary.wiley.com/doi/pdf/10.1029/2011PA002158) 803 doi: https://doi.org/10.1029/2011PA002158 804
- Shaari, H. b., Yamamoto, M., & Irino, T. (2013, September). Enhanced upwelling in 805
- the eastern equatorial Pacific at the last five glacial terminations. Palaeogeog-806
- Retrieved 2021-05-12, raphy, Palaeoclimatology, Palaeoecology, 386, 8–15. 807
- from https://www.sciencedirect.com/science/article/pii/
- S0031018213001600 doi: 10.1016/j.palaeo.2013.03.022 809
- Shi, H., García-Reyes, M., Jacox, M. G., Rykaczewski, R. R., Black, B. A., Bograd, S. J.,
- & Sydeman, W. J. Co-occurrence of california drought and northeast pa-(2021).811
- cific marine heatwaves under climate change. Geophysical Research Letters, 48(17), 812
- e2021GL092765. 813
- Sniderman, J., Brown, J. R., Woodhead, J. D., King, A. D., Gillett, N. P., Tokarska, K. B., 814
- ... Meinshausen, M. (2019). Southern Hemisphere subtropical drying as a transient 815
- response to warming. Nature Climate Change, 9(3), 232–236.
- Tierney, J. E., Haywood, A. M., Feng, R., Bhattacharya, T., & Otto-Bliesner, B. L. (2019).
- Pliocene warmth consistent with greenhouse gas forcing. Geophysical Research Let-
- ters, 46(15), 9136–9144. 819
- Tierney, J. E., Pausata, F. S., & deMenocal, P. B. (2017). Rainfall regimes of the green sahara. Science advances, 3(1), e1601503. 821
- Tierney, J. E., & Tingley, M. P. (2018). BAYSPLINE: A new calibration for the alkenone pa-822 leothermometer. Paleoceanography and Paleoclimatology, 33(3), 281–301. 823
- Wheeler, L. B., Galewsky, J., Herold, N., & Huber, M. (2016). Late cenozoic surface uplift 824 of the southern sierra nevada (california, usa): A paleoclimate perspective on lee-side 825 stable isotope paleoaltimetry. Geology, 44(6), 451–454.
- 826
- Williams, A. P., Cook, B. I., & Smerdon, J. E. (2022). Rapid intensification of the emerging 827 southwestern North American megadrought in 2020–2021. Nature Climate Change, 828
- 1-3.829
- Windler, G., Tierney, J. E., & Anchukaitis, K. J. (2021). Glacial-interglacial shifts dominate 830 tropical indo-pacific hydroclimate during the late pleistocene. Geophysical Research
- Letters, 48(15), e2021GL093339.
- Xie, S.-P., Deser, C., Vecchi, G. A., Ma, J., Teng, H., & Wittenberg, A. T. (2010).
- warming pattern formation: Sea surface temperature and rainfall. Journal of Climate, 834
- 23(4), 966-986. 835
- (2017).Yang, L., Smith, J., Baeck, M. L., Morin, E., & Goodrich, D. C. Flash flooding 836
- in arid/semiarid regions: Dissecting the hydrometeorology and hydrology of the 19 837
- August 2014 storm and flood hydroclimatology in Arizona. Journal of Hydrometeorol-838

ogy, 18(12), 3103-3123. 839 Zappa, G., Ceppi, P., & Shepherd, T. G. (2020). Time-evolving sea-surface warming patterns 840 modulate the climate change response of subtropical precipitation over land. Proceed-841 ings of the National Academy of Sciences, 117(9), 4539-4545. 842 Zaytsev, O., Cervantes-Duarte, R., Montante, O., & Gallegos-Garcia, A. (2003).Coastal upwelling activity on the Pacific shelf of the Baja California Peninsula. Journal of oceanography, 59(4), 489-502. 845 Zhu, J., Poulsen, C. J., & Tierney, J. E. (2019). Simulation of Eocene extreme warmth and 846 high climate sensitivity through cloud feedbacks. Science advances, 5(9), eaax1874. 847 Zhu, Y., Zhang, R.-H., & Sun, J. (2020, September). North Pacific Upper-Ocean Cold 848 Temperature Biases in CMIP6 Simulations and the Role of Regional Vertical 849 *Journal of Climate*, *33*(17), 7523–7538. Retrieved 2021-12-20, from 850 https://journals.ametsoc.org/view/journals/clim/33/17/ 851

jcliD190654.xml doi: 10.1175/JCLI-D-19-0654.1

AGU ADVANCES

Supporting Information for "Expansion and intensification of the North American Monsoon during the Pliocene"

Tripti Bhattacharya ¹, Ran Feng ², Jessica E. Tierney ³, Claire Rubbelke ¹, Natalie Burls ⁴, Scott Knapp ⁴, Minmin Fu ⁵

 $^{1}\mathrm{Department}$ of Earth and Environmental Sciences, Syracuse University, Syracuse NY

 $^2\mathrm{Department}$ of Geosciences, University of Connecticut, Storrs CT

³Department of Geosciences, University of Arizona, Tucson AZ

⁴Department of Atmospheric, Oceanic and Earth Sciences, George Mason University, Fairfax VA

 5 Department of Earth and Planetary Sciences, Harvard University, Cambridge, MA

Contents of this file

- 1. Text S1
- 2. Text S2
- 3. References
- 4. Tables S1 to S4
- 5. Figures S1 to S6

X - 2 :

Text S1 - Detailed Methods

iCAM5 Simulations with Fixed SSTs

To establish a linkage between precipitation isotopes, monsoon rainfall, and SST changes, we performed a simulation with the isotopologue-tracking enabled Community Earth System Model 1.2 (iCESM1.2) in atmosphere-only mode (e.g. iCAM5) (Brady et al., 2019). The atmospheric model is run at a 0.9° x1.25° horizontal resolution, with 30 vertical layers. While isotope-enabled models have limitations, we note that the pre-industrial simulation of iCAM5 used in this study is able capture the seasonal contrast in precipitation δ D found in GNIP station data in Tucson AZ, with an enriched summer monsoon compared to depleted winter rainfall (Figure S6), despite the fact that iCESM1.2's rainfall isotopes are depleted compared to observations at Tucson's GNIP station (Nusbaumer et al., 2017). In addition, iCAM5 performs slightly better than other models at simulating rainfall isotope changes due to changing stratiform fraction (Hu et al., 2018). We therefore suggest that this model is appropriate for investigating changes in δ D_p associated with Pliocene boundary conditions.

We perform one simulation using the SST field from Fu, Cane, Molnar, and Tziperman (2022), which uses reconstructed Pliocene SSTs with amplified warming on the southern California Margin. SSTs used in this simulation are shown in Figure S5, panel a. This simulation is used to diagnose the linkage between SST changes, δD_p , and summer rainfall. In this simulation, we analyze isotopes of water vapor and precipitation, and plot changes in precipitation, winds, as well as derived fields like equivalent potential temperature (θ_e).

To identify the influence of different SST patterns on NAM strength, we perform a set of 7 additional sensitivity experiments using iCAM5 with prescribed SST fields. All

: X - 3

simulations use the same Pliocene boundary conditions adapted for Community Earth System Model, and use CO₂ concentrations of 400 ppm (Feng et al., 2020). These contrast with the simulation with SSTs from Fu et al. (2022), which used modern boundary conditions. Of the sensitivity experiments, two experiments were designed analyze the impact of uniform warming. SSTs in these experiments are increased by 1°C and 2°C without any changes in spatial patterns (Table S4). The 1°C warming field is shown in Figure S5, panel b. This means that this experiment represents a uniform warming of 1°C on top of the SST anomalies from a coupled CESM1.2 simulation from (Feng et al., 2020).

Four of the experiments are designed to sample a range of SST gradient changes associated with CA coastal warming. The coastal warming pattern is derived from the pattern of North Pacific ocean-wide SST anomalies during the 2014 western U.S. coast marine heat wave event. In order to create prescribed SSTs for the iCAM5 simulations, these SST anomalies were scaled by 1x, 2x, 3x, and 4x and added to Pliocene SST field obtained from a fully-coupled model simulations using the Community Earth System Model version 1.2 (CESM1.2) using the same boundary conditions (Feng et al., 2020). The 1x pattern from these 'MHW-like' experiments is shown in Figure S5, panel c. All experiments were run for 40 model years. The last 20 model years are averaged to produce climatologies. For clarity, Table S4 details each experiment's SST design, how CA margin and the subtropical/tropical gradient vary across simulations.

Text S2 - Interpretation of Inferred δD_p

Plio-Pleistocene changes in leaf wax isotopes reflect changes in the intensity and spatial extent of moist convection over southern California and Baja California. Modern core-

X - 4

top samples show a more enriched value of δD_p in the southern Gulf of California, where monsoonal, convective rainfall forms a greater proportion of total rainfall (Figure S2). Seasonal changes in precipitation isotopes, measured at a GNIP station in Tucson, also suggest that the summer months, which feature more convective rainfall, have a more enriched isotopic signature (Figure S2) (Bhattacharya et al., 2018).

Monsoon rainfall is characterized by a greater proportion of deep convection, and exhibits a more positive value of δD_p . Deep convective monsoon rainfall results from ice hydrometeors that develop when vapor evaporated in a warm, saturated boundary layer is lifted in strong updrafts, resulting in a more enriched isotopic signature for rainfall (Aggarwal et al., 2016). In contrast, stratiform rainfall tends to form in environments with relatively weak updrafts, and may develop relatively slowly, incorporating mid to upper tropospheric water vapor and undergoing more phase changes, resulting in a depleted isotopic signature (Aggarwal et al., 2016). This is opposite to the 'amount effect,' where more rainfall is associated with a more depleted isotopic signature (Risi et al., 2008), but is consistent with our understanding of regional isotope systematics. The NAM region differs from other tropical regions (e.g. the Asian monsoon) as it receives a substantial amount of stratiform rainfall, which likely overprints any amount effect (Schumacher & Houze, 2003). Other processes, like temperature and changes in vapor source region, may influence inferred δD_p values. However, equilibrium temperature effects (e.g. changes in the fractionation between atmospheric water vapor and rainfall) could only account for 5-7% of the overall change observed in δD_p values at most. SST anomalies between 3.5 and 3.0 Ma at DSDP 475 and ODP 1012 were between 4-6°C warmer than pre-industrial values, which would translate into a 4 to 6 \% change in δD_p relative to atmospheric wa: X - 5

ter vapor, assuming that condensation temperatures shifted similarly to SSTs. This is smaller than the magnitude of δD_p change at both sites, suggesting other processes are responsible for the full magnitude of the signal.

References

- Adler, R. F., Sapiano, M. R., Huffman, G. J., Wang, J.-J., Gu, G., Bolvin, D., . . . others (2018). The Global Precipitation Climatology Project (GPCP) monthly analysis (new version 2.3) and a review of 2017 global precipitation. *Atmosphere*, 9(4), 138.
- Aggarwal, P. K., Romatschke, U., Araguas-Araguas, L., Belachew, D., Longstaffe, F. J., Berg, P., . . . Funk, A. (2016). Proportions of convective and stratiform precipitation revealed in water isotope ratios. *Nature Geoscience*, 9(8), 624–629.
- Ballog, R. A., & Malloy, R. E. (1981). Neogene Palynology from the Southern California

 Continental Borderland, Site 467, Deep Sea Drilling Project Leg 64 (Vol. 63). U.S.

 Government Printing Office.
- Bhattacharya, T., Tierney, J. E., Addison, J. A., & Murray, J. W. (2018). Ice-sheet modulation of deglacial North American monsoon intensification. *Nature Geoscience*, 11(11), 848–852.
- Brady, E., Stevenson, S., Bailey, D., Liu, Z., Noone, D., Nusbaumer, J., . . . others (2019).

 The connected isotopic water cycle in the Community Earth System Model version

 1. Journal of Advances in Modeling Earth Systems, 11(8), 2547–2566.

X - 6 :

- Eastoe, C., & Dettman, D. (2016). Isotope amount effects in hydrologic and climate reconstructions of monsoon climates: Implications of some long-term data sets for precipitation. *Chemical Geology*, 430, 78–89.
- Feng, R., Otto-Bliesner, B. L., Brady, E. C., & Rosenbloom, N. (2020). Increased climate response and earth system sensitivity from ccsm4 to cesm2 in mid-pliocene simulations. *Journal of Advances in Modeling Earth Systems*, 12(8), e2019MS002033.
- Fu, M., Cane, M. A., Molnar, P., & Tziperman, E. (2022, January). Warmer Pliocene upwelling site SST leads to wetter subtropical coastal areas: a positive feedback on SST. Paleoceanography and Paleoclimatology, e2021PA004357.
- Hu, J., Emile-Geay, J., Nusbaumer, J., & Noone, D. (2018). Impact of convective activity on precipitation δ 180 in isotope-enabled general circulation models. *Journal of Geophysical Research: Atmospheres*, 123(23), 13–595.
- Ibarra, D. E., Oster, J. L., Winnick, M. J., Caves Rugenstein, J. K., Byrne, M. P., & Chamberlain, C. P. (2018). Warm and cold wet states in the western United States during the Pliocene–Pleistocene. *Geology*, 46(4), 355–358.
- Miller, W. E. (1980). The late Pliocene Las Tunas local fauna from southernmost Baja California, Mexico. *Journal of Paleontology*, 762–805.
- Nusbaumer, J., Wong, T. E., Bardeen, C., & Noone, D. (2017). Evaluating hydrological processes in the C ommunity A tmosphere M odel V ersion 5 (CAM5) using stable

X - 7

isotope ratios of water. Journal of Advances in Modeling Earth Systems, 9(2), 949–977.

- Remeika, P., Fischbein, I. W., & Fischbein, S. A. (1988). Lower Pliocene petrified wood from the Palm Spring Formation, Anza Borrego Desert State Park, California.

 Review of palaeobotany and palynology, 56(3-4), 183–198.
- Risi, C., Bony, S., & Vimeux, F. (2008). Influence of convective processes on the isotopic composition (δ18O and δD) of precipitation and water vapor in the tropics:
 2. Physical interpretation of the amount effect. Journal of Geophysical Research:
 Atmospheres, 113(D19).
- Schumacher, C., & Houze, R. A. (2003). The TRMM precipitation radar's view of shallow, isolated rain. *Journal of Applied Meteorology and Climatology*, 42(10), 1519–1524.

X - 8

 ${\bf Table~S1.} \quad {\bf Locations~and~interpretations~of~Pliocene~data~shown~in~Figure~1}$

Site	Name	Lat	Lon	Age (Ma)	Interpretation	Source
1	Diablo Formation	33.26	-116.37	3.8 - 2.6	mesic plant taxa incl Juglans, Carya, Umbellu- laria, Populus	(Remeika et al., 1988)
2	DSDP 467	33.83	-120.75	15 - 2.4	Carya, Juglans indicate summer wet to summer dry transition	(Ballog & Malloy, 1981)
3	Las Tunas	23.3	-109.7	4.75 - 2.6	faunal remains incl. and tortoise indicate perennial freshwater, tropical envi- ronment	(Miller, 1980)
4	Palm Springs	33.57	-115.85	3.3 - 2.6	Lacustrine Deposits	Macrostrat, (Ibarra et al., 2018)
5	Gila Conglomerate	32.48	-108.26	4.0 - 2.6	Lacustrine Deposits	Macrostrat, (Ibarra et al., 2018)
6	Fort Hancock	31.91	-106.5	3.6 - 1.9	Lacustrine Deposits	Macrostrat, (Ibarra et al., 2018)
7	Santa Fe Group 1	33.05	-105.61	19.3 - 1.9	Lacustrine Deposits	Macrostrat, (Ibarra et al., 2018)
8	Santa Fe Group 2	34.15	-107.28	4.9 - 0.7	Lacustrine Deposits	Macrostrat, (Ibarra et al., 2018)
9	Sunshine Ranch/Saugus Fm	34.3	-118.53	3.1 - 2.8	Lacustrine Deposits	Macrostrat, (Ibarra et al., 2018)
10	Hueca Bolson, TX	30.90	-105.30	4.75 - 1.8	Lacustrine Deposits	Macrostrat, (Ibarra et al., 2018)
11	Hungry Valley	34.67	-118.66	4.9 - 2.6	Lacustrine Deposits	Macrostrat, (Ibarra et al., 2018)
12	Paso Robles	36.5	-121.74	1.9-8.3	Lacustrine Deposits	Macrostrat, (Ibarra et al., 2018)
13	Bidahochi	35.95	-109.91	5.3-2.6	Lacustrine Deposits	Macrostrat, (Ibarra et al., 2018)

: X - 9

Table S2. Individual plant taxa from the Arizona-Sonora Desert Museum of δD_{wax} and $\delta^{13}C_{wax}$ for C_4 monocots/grasses and C_3 eudicots used to infer ε_{p-w} . Values are for the C_{30} fatty acid. Graminoids/grasses are marked with an asterisk (*).

Taxon	Ecosystem	Metabolism	$\delta^{13}\mathbf{C}_{wax}$ (%VPDB)	$\delta \mathbf{D}_{wax}$ (%VSMOW)
$Acacia\ will ardiana$	Thornscrub	C_3	no data	-97
$Ambrosia\ ambrosoides$	Sonoran Desert	C_3	-35.7	-126
$Ambrosia\ cordifolia$	Sonoran Desert	C_3	-37.5	-115
$Ambrosia\ delto idea$	Sonoran Desert	C_3	-31.8	-116
$Aristida\ ternipes*$	Sonoran Desert	C_4	-29.1	-158
$Brongniartia\ tenuifolia$	Thornscrub	C_3	no data	-124
$Bursera\ laxiflora$	Thornscrub	C_3	no data	-151
$Bursera\ microflora$	Thornscrub	C_3	no data	-132
$Cathestecum\ brevifolum*$	Sonoran Desert	C_4	-27.1	-164
$Dy schoriste\ hir sut is sima$	Thornscrub	C_3	no data	-137
$Encelia\ farinosa$	Sonoran Desert	C_3	-30.9	-149
$Eupatorium\ sagittatum$	Sonoran Desert	C_3	no data	-142
$Chromolaena\ sagittata$	Thornscurb	C_3	no data	-145
$For chhammeria\ watsonii$	Thornscrub	C_3	no data	-90
$Fou queria\ macdougalii$	Thornscrub	C_3	no data	-143
$Guaiacum\ coulteri$	Thornscrub	C_3	no data	-113
$Hae matoxylon\ brasilleto$	Thornscrub	C_3	-34.8	-126
Henrya insularis	Thornscrub	C_3	no data	-145
$Ipomnea\ arborescens$	Thornscrub	C_3	no data	-126
$Jacquinia\ macrocarpa$	Thornscrub	C_3	no data	-157
$Jatropha\ cartiophylla$	Sonoran Desert	C_3	-30.1	-179
$Larrea\ tridentata$	Sonoran Desert	C_3	-31.7	-116
$Melochia\ tomentosa$	Thornscrub	C_3	no data	-155
$Muhlenbergia\ porterii*$	Sonoran Desert	C_4	-26.5	-162
$Olneya\ tesota$	Sonoran Desert	C_3	-30.1	-111
$Parkinsonia\ microphylla$	Sonoran Desert	C_3	-31.9	-156
$Piscidia\ mollis$	Sonoran Desert	C_3	no data	-149
$Prosopis\ velutina$	Sonoran Desert	C_3	no data	-106
$Randia\ echinocarpa$	Sonoran Desert	C_3	no data	-119
$Simmondsia\ chinensis$	Sonoran Desert	C_3	-31.8	-134
$Solanum\ tridynamum$	Thornscrub	C_3	no data	-150
$Trixis\ californica$	Sonoran Desert	C_3	-37.2	-138
$Vachellia\ campechiana$	Thornscrub	C_3	no data	-119
$Vachellia\ constricta$	Thornscrub	C_3	-37.1	-105

X - 10

Table S3. End-members of δ^{13} C and ε_{p-w} used for our calculation of leaf wax-inferred δD_p . δ^{13} C values have been corrected for the Suess effect. All carbon end-members come from modern plants at the Arizona-Sonora Desert Museum

Value	Mean	Standard Error	Sample Size
$\delta^{13}C_3$ (Eudicots)	-32.1	0.7	12
$\delta^{13}C_4$ (Graminoids)	-26.5	2.3	3
ε_{C4} (Eudicots)	-113	3	3
ε_{C3} (Graminoids)	-81	4	31

Table S4. Overview of iCAM5 simulations used in this study, along with the response they identify (see Text S1). Simulations include an idealized SST run following Fu et al. (2022), as well as six sensitivity experiments.

Experiment	Description	Response	
Pliocene SSTs	SST pattern from (Fu et al., 2022)	Hydroclimate response to Pliocene SSTs	
1°C Uniform	$1^{\circ}\mathrm{C}$ warming + CESM1.2 coupled SSTs	Uniform warming with no pattern change	
2°C Uniform	$2^{\circ}\mathrm{C}$ warming + CESM1.2 coupled SSTs	Uniform warming with no pattern change	
1x MHW	1x MHW pattern + CESM1.2 coupled SSTs	Amplified Subtropical warming relative to EEP	
2x MHW	2x MHW pattern + CESM1.2 coupled SSTs	Amplified Subtropical warming relative to EEP	
3x MHW	3x MHW pattern + CESM1.2 coupled SSTs	Amplified Subtropical warming relative to EEP	
4x MHW	4x MHW pattern + CESM1.2 coupled SSTs	Amplified Subtropical warming relative to EEP	

: X - 11

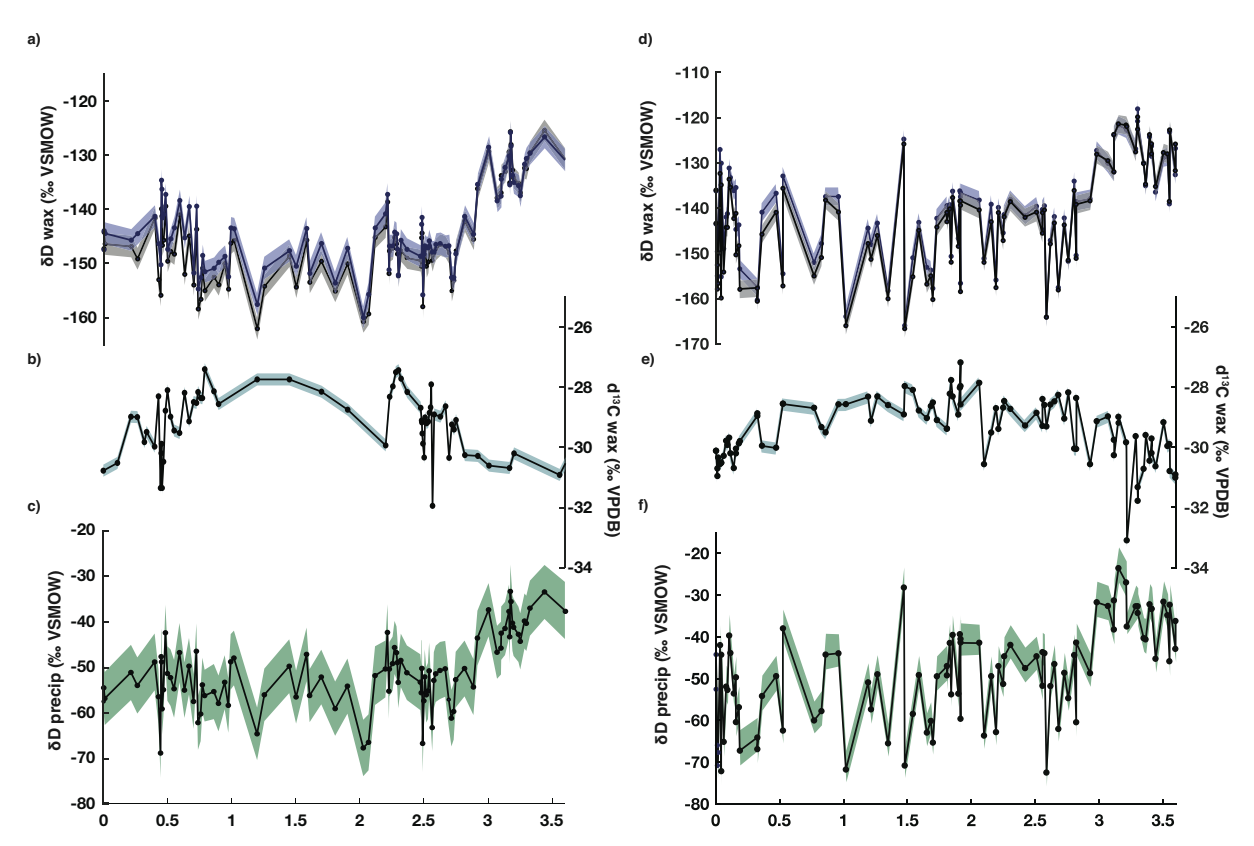


Figure S1. C_{30} alkanoic acid δD , $\delta^{13}C$, and inferred δD_p from sites DSDP 475 (left) and ODP 1012 (right). All values are shown with 1σ uncertainties. a) and d) show δD of the C_{30} alkanoic acid, with gray curve reflecting ice-volume corrected values. The effect of a million-year ice volume correction is extremely minor. b) and e) show carbon isotope data with 1σ analytical error. At site 475, carbon isotopes were analyzed at a lower resolution since for several depths sample material was consumed for hydrogen isotope analysis. c) and f) show inferred δD_p values for each site. Note the larger uncertainty that includes analytical uncertainty and uncertainty from the Bayesian mixing model.

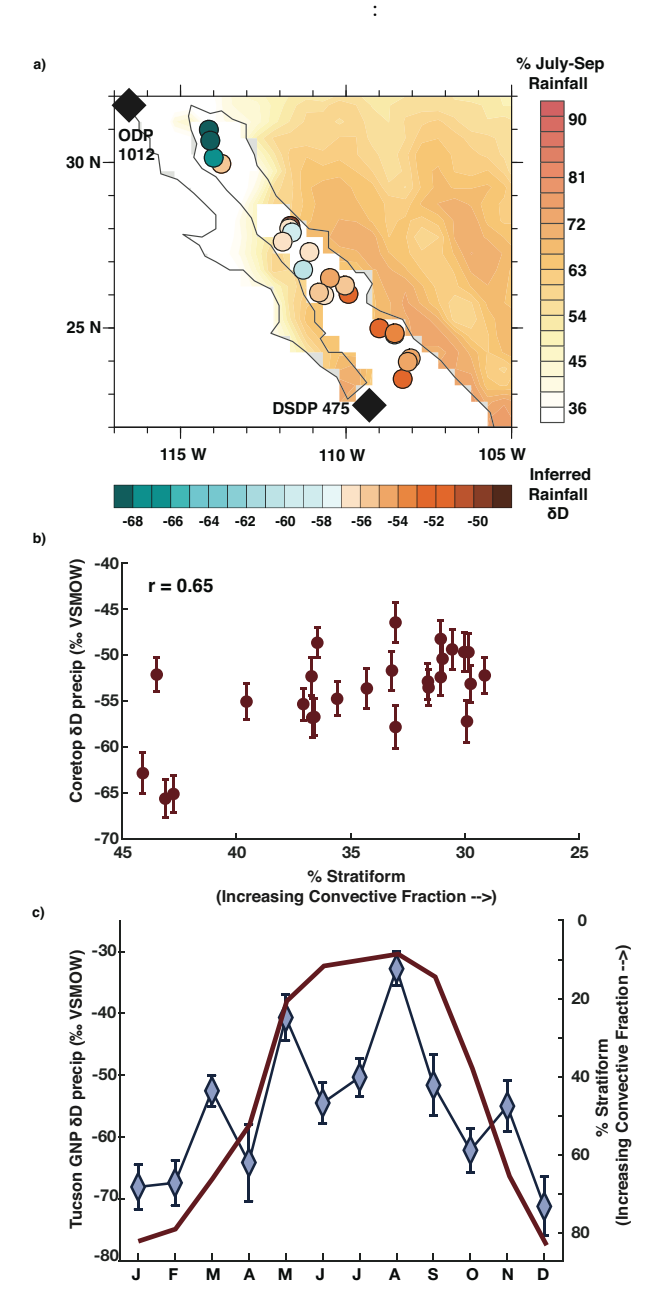


Figure S2. a) Coretop-inferred δD_p in the Gulf of California from Bhattacharya et al. (2018). Original data are replotted using updated $\delta^{13}C$ and ε_{p-w} corrections from Table S2. Background contours indicate the percentage of NAM contribution to annual rainfall. b) Coretop δD_p plotted against the percentage of rainfall on adjacent land regions that derives from stratiform rainfall (decreasing stratiform fraction indicates a greater share of convective precipitation). Stratiform fraction is used following the convention of Aggarwal et al. (2016). c) Seasonal cycle in Tucson GNIP station (Eastoe & Dettman, 2016) δD_p versus percent stratiform rainfall.

September 27, 2022, 2:28pm

: X - 13

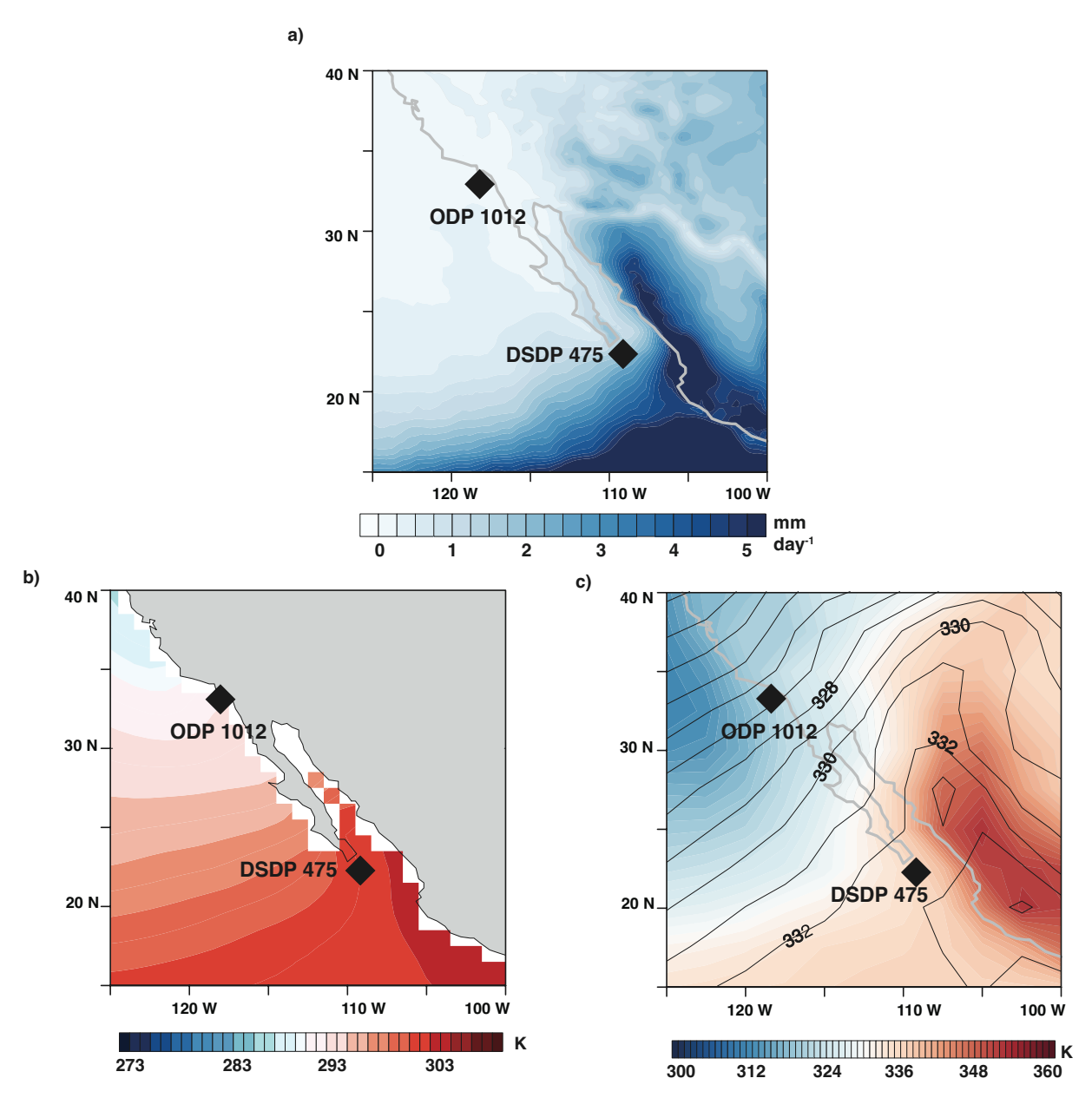


Figure S3. July-September climatology, calculated from 1950 - 2018, of a) rainfall in mm/day, b) sea surface temperatures, and c) equivalent potential temperature or θ_e (solid contours are mid-tropospheric or 400 mb θ_e , while colored contours are low-level (surface to 900 mb) average θ_e). The location of DSDP 475 and ODP 1012 is indicated on each plot.

X - 14

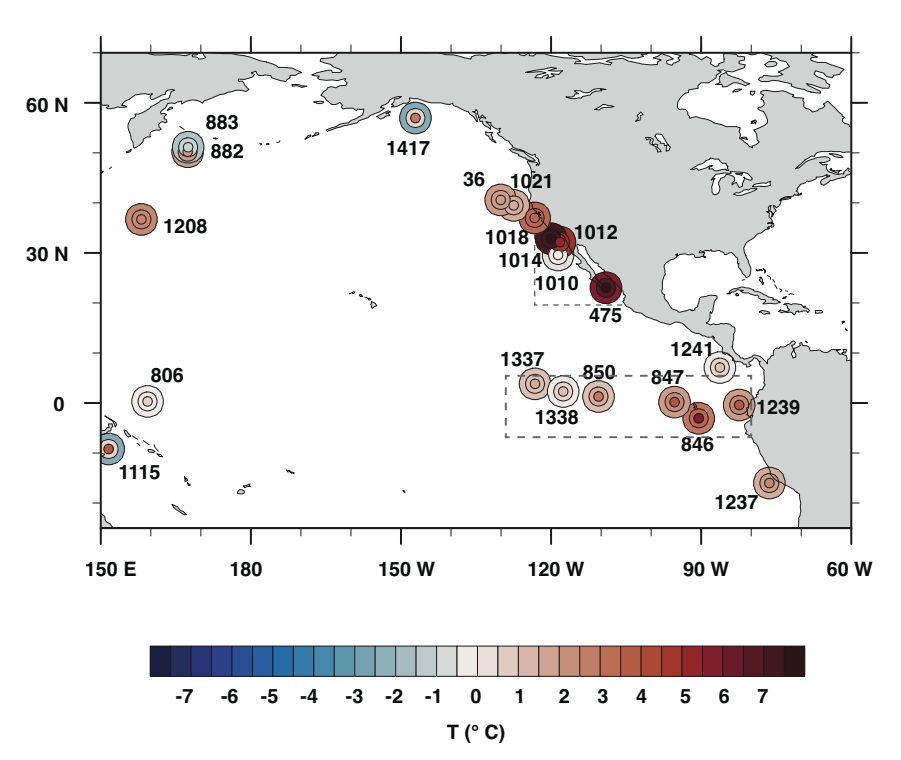


Figure S4. Mid-Pliocene (3.3 to 3.0 Ma) SST anomalies in alkenone-based temperature records across the north Pacific. Inner circle represents upper 95% confidence interval, middle circle is median value, while outer circle is the lower 95% confidence interval of ensemble estimates with analytical and calibration errors propagated through the timeseries. Regions used to create averages of subtropical eastern Pacific (southern California Margin) and eastern equatorial Pacific SSTs are outlined in dashed rectangles.

: X - 15

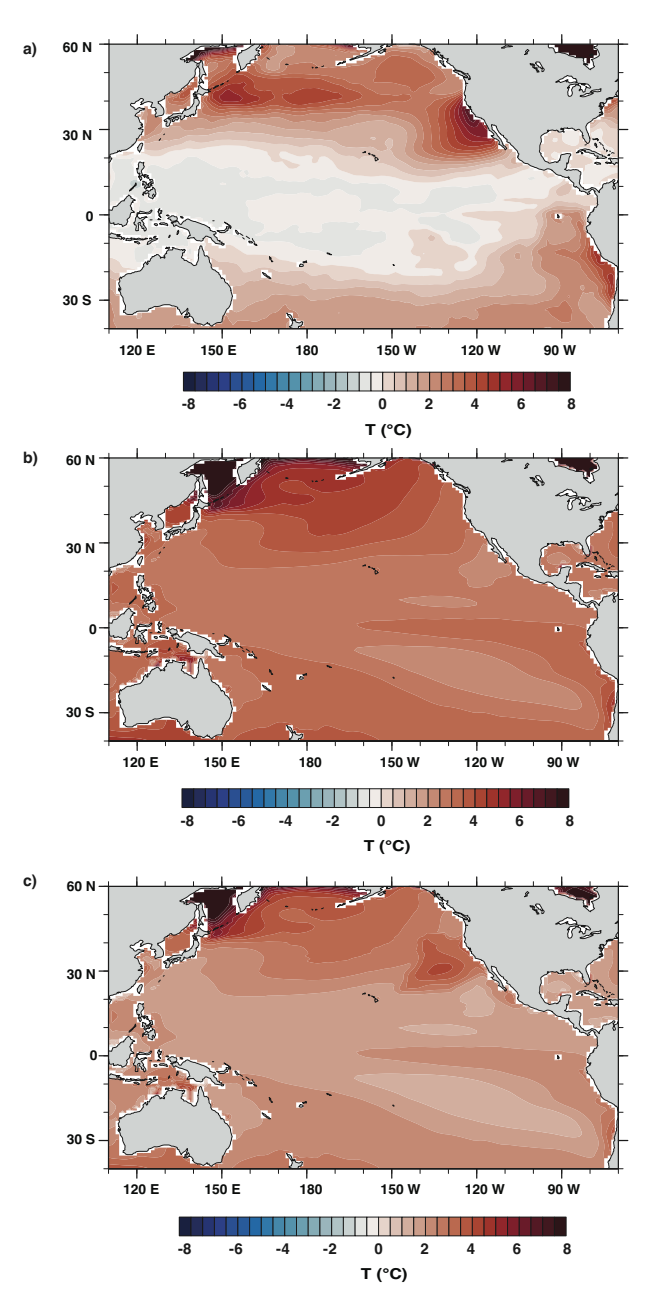


Figure S5. SST fields used for the iCAM5 simulations (see section 1 and Table S4. a) SSTs from Fu et al. (2022), which are also shown in Figure 2 in the main text. b) SSTs from a global 1 degree warming simulation. c) SST pattern with amplified coastal warming (taken from the 2014 marine heat wave). In Figure 3, we show results from iCAM5 simulations using 1x and 2x the warming pattern shown in panel b), as well as results from iCAM5 forced with 1x, 2x, 3x, and 4x the pattern in panel c).

X - 16 :

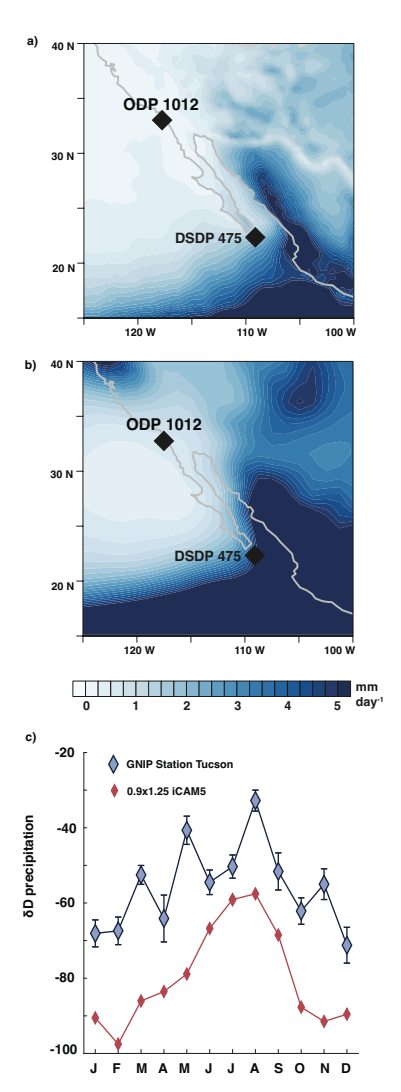


Figure S6. Observational vs. iCAM5 climatology for rainfall and the seasonal cycle of isotopes. a)GPCP July-September rainfall (Adler et al., 2018). b) Model climatology for the same interval. c) Climatology and standard error of measured precipitation δD from the Tucson GNIP station (Eastoe & Dettman, 2016) in dark blue compared to iCAM5's precipitation climatology for a region surrounding Tucson in red.